RSC Advances

PAPER

View Article Online
View Journal | View Issue

Cite this: *RSC Adv.*, 2025, **15**, 19530

Impact of trifluoromethyl Ugi adducts as anticancer agents: EGFR inhibition, apoptosis induction and miRNA up-regulation †

Mohammed Salah Ayoup, *[a] Eman Mamdouh,[b] Saied M. Soliman,[b] Ibrahim Elghamry,[a] Mohamed S. Nafie,[cd] Amr Negm,[a] Amr Sonousi,[ef] Asmaa E. Kassab[e] and Laila F. Awad*[b]

A series of novel bis-amide Ugi adducts with a Y-shaped configuration imitating the thematic feature of fourth-generation EGFR inhibitors was designed and synthesized *via* a one-step Ugi four-component reaction. All the synthesized Ugi adducts were evaluated for their anti-proliferative efficacy against MDA-MB-231 human breast cancer and A549 non-small cell lung cancer cell lines. Their selectivity was assessed using normal human lung epithelial cells (BEAS-2B). The Ugi adduct **5** stood up as the study hit concerning cytotoxic efficacy and selectivity. It was 1.42- and 1.20-fold more potent than 5-FU and cisplatin, respectively, against the MDA-MB-231 cell line, and 1.82- and 1.62-fold more potent than 5-FU and cisplatin, respectively, against the A549 cell line. Additionally, compound **5** demonstrated the most prominent selectivity against MDA-MB-231 and A549 cells (SI = 7 and 11.7, respectively); it was 14 to 20.9-fold safer than 5-FU and cisplatin. Accordingly, it was subjected to further enzymatic and mechanistic studies. The Ugi adduct **5** showed excellent sub-micromolar potency (IC_{50} = 0.19 μM) against human mutant $EGFR^{T790M/C797S/L858R}$ enzyme equipotent with that of osimertinib (IC_{50} = 0.1 μM). It exhibited a promising IC_{50} value of 2.1 nM against the $EGFR^{WT}$ enzyme, comparable to erlotinib (IC_{50} = 1.3 nM). In comparison to the untreated control, the Ugi adduct **5** caused a decrease in the expression of the cancer initiation, angiogenic, and metastatic markers (c-Myc, CD-44, CD-133, VEGF, and TGF) to 0.36, 0.5, 0.7, 0.5, and 0.4-fold, respectively, in MDA-MB-231 cells. Regarding A549 cells, the exposure to compound **5** showed a 0.41, 0.64, 0.58, 0.71, and 0.69-fold reduction in the expression of c-Myc, CD-44, CD-133, VEGF, and TGF markers compared to the untreated control. Compound **5** markedly elevated miRNA-132 and miRNA-200c expressions in the MDA-MB-231 cell line by 3.8 and 3.1-fold, while in A549 cells, compound **5** demonstrated enhancement of miRNA-132 and miRNA-200c expression by 2.4 and 1.9-fold changes compared to that of the control. It promoted apoptosis induction *via* caspase 3/9 activation (1.8 and 2.3-folds) in the A549 cell line. The molecular docking interpretations of the most potent Ugi adduct **5** in $EGFR^{L858R/T790M/C797S}$ (PDB ID: 6LUB) and the wild-type $EGFR^{WT}$ (PDB ID: 1M17) enzymes are aligned with and explain its potential to dually inhibit $EGFR^{L858R/T790M/C797S}$ and $EGFR^{WT}$ tyrosine kinases.

Received 27th February 2025
Accepted 22nd May 2025

DOI: 10.1039/d5ra01428j

rsc.li/rsc-advances

1. Introduction

Cancer continues to rank among the most serious public health concerns, with its incidence and mortality rates continuing to place a heavy strain on healthcare systems and populations worldwide. In the 21st century, cancer is a significant social, public health, and financial issue.[1,2] Three out of every ten premature deaths (people 30–69 years old) worldwide are caused by cancer, and in 177 out of 183 countries, it is one of the top three causes of death in this age group.[3] In 2022, about 20 million new cases of cancer, 9.7 million deaths, and 53.5 million prevalent cases are estimated by the Global Cancer Observatory of the International Agency for Research on Cancer (IARC).[4]

[a]*Department of Chemistry, College of Science, King Faisal University, Al-Ahsa 31982, Saudi Arabia. E-mail: mayoup@kfu.edu.sa; mohammedsalahayoup@gmail.com*
[b]*Chemistry Department, Faculty of Science, Alexandria University, P. O. Box 426, Alexandria, 21321, Egypt. E-mail: laila.fathy@yahoo.com*
[c]*Department of Chemistry, College of Sciences, University of Sharjah, Sharjah 27272, United Arab Emirates*
[d]*Chemistry Department, Faculty of Science, Suez Canal University, Ismailia 41522, Egypt*
[e]*Department of Pharmaceutical Organic Chemistry, Faculty of Pharmacy, Cairo University, Kasr El-Aini Street, P. O. Box 11562, Cairo, Egypt*
[f]*University of Hertfordshire Hosted By Global Academic Foundation, New Administrative Capital, Cairo, Egypt*

† Electronic supplementary information (ESI) available. See DOI: https://doi.org/10.1039/d5ra01428j

Most cancers are caused by genetic defects; mutations can give normal cells new characteristics that cause them to become malignant. The capacity of cancer cells to invade and spread is one of the characteristics of the disease that are determined by genome instability and mutations.[5] A cancerous cell can move inside tissues due to its ability to migrate and invade those tissues. These activities enable cancerous cells to spread across the blood and lymphatic vessels, disseminate throughout the body, and then proliferate metastatically in other organs.[6] One of the main causes of death for breast and lung cancer patients and a defining feature of the disease is metastasis.[5] Malignant cells leave the primary site and travel throughout the body during the metastasis process, creating secondary sites and seriously impairing organ function.[7]

Thus, in its most aggressive form, cancer is a disease of unchecked cell migration as well as unchecked cell growth. Metastasis requires a sequence of intricate steps known as the "metastatic cascade". It is triggered by the initiation of tumor growth and angiogenesis, followed by cell migration and intravasation. Invasion is from the initial stages of the metastatic cascade, as cancer cells penetrate the basement membrane and move into the surrounding tissue through the extracellular matrix.[8,9] The identification of therapeutics that co-target cancer cell proliferation, invasion, and migration pathways may provide novel treatment regimens for cancer patients.

The primary player in growth factor signaling is the epidermal growth factor receptor (EGFR). The receptor and the tyrosine kinase comprise the two functional domains of the EGFR. *Via* intracellular signal transduction, EGFR is necessary for regular cellular regulation and delivers extracellular signals into cells across the cell membrane.[10,11]

Overexpression and abnormal signaling of this receptor increase downstream consequences like angiogenesis, cell survival, and proliferation, eventually resulting in unchecked cell growth, differentiation, neovascularization, metastasis, and resistance of cancer cells.[12,13]

The majority of solid tumors, including breast, colon, and lung cancers, have been shown to exhibit abnormal overexpression (up to 20 times the expression of EGFR in normal cells) in addition to EGFR mutations, which are linked to a poor prognosis, so EGFR is a potential molecular therapeutic target for anticancer candidates.[14–17] Gefitinib (Iressa TM)[18] and erlotinib (Tarceva TM)[19] (Fig. 1) with 4-anilinoquinazoline motifs are reversible inhibitors of the first generation of EGFR tyrosine kinase inhibitors (TKIs) that specifically block EGFR (Erb-B1) signaling as an EGFR subtype. They potentially treat cancer patients with EGFR overexpression, and they initially produce good responses. Most of these patients develop resistance to this class within a year because of the EGFR T790M mutation.[20,21]

Afatinib and dacomitinib (Fig. 1), quinazoline-based irreversible inhibitors, have been developed as second-generation EGFR inhibitors to counteract the EGFR T790M mutation caused by gefitinib or erlotinib.[22,23] One of these compounds' structural characteristics is the γ-amino acrylamide framework, which can function as a Michael acceptor to create irreversible covalent bonds with the SH group in the Cys797 residue at the edge of the ATP binding pocket of the receptor. On the other hand, irreversible inhibitors exhibit strong efficacy against normal cell-found $EGFR^{WT}$ (wild type),[24] and therefore, the usage of dosages that would be required to adequately suppress T790M is prohibited due to the toxicity (interstitial lung disease, rash, and diarrhea) that results from blocking wild-type EGFR.

To target mutant EGFR containing T790M, third-generation EGFR TKIs have recently been developed, including osimertinib (Tagrisso TM) (Fig. 1), olmutinib, naquotinib, and avitinib.[25–28] This class spares the wild-type EGFR in favor of acting only on EGFR mutations, especially osimertinib, which was approved by the Food and Drug Administration (FDA) in 2015 to treat patients with non-small cell lung cancer (NSCLC) who have EGFR-activating mutations, such as the L858R point mutation or in-frame deletions of exon 19, and the EGFR T790M mutation.[29] Resistance develops quickly once osimertinib is administered to patients with EGFR T790M mutation, usually throughout nine to thirteen months due to the activation of other resistance mechanisms, incorporating the C797S point mutation into serine that can obstruct the formation of covalent bonds with irreversible EGFR inhibitors, hence significantly lowering the therapeutic activity.[30–32]

Fourth-generation EGFR inhibitor design strategies have significantly evolved to target the T790M mutation and other resistant variations, like C797S, with an emphasis on Y-shaped designs and other molecular configuration changes. Y-shaped structures can accommodate a variety of mutations, including C797S and T790M, by interacting with distinct sub-pockets and inducing an inactive conformation of the receptor. Because of the adaptable design of Y-shaped EGFR inhibitors, they can effectively combat complicated resistance mutations like T790M/C797S. The arms of Y-shaped inhibitors are bifurcated and extend into different EGFR kinase domain sub-pockets, ensuring improved adaptability in targeting various sites, which qualifies them for conquering acquired resistance. Additionally, this configuration ensures effective binding by successfully addressing the steric barrier brought on by the large T790M residue. This design provides a wider binding profile, which guarantees interactions with the hinge region and solvent-exposed portions. By distinguishing between mutant and wild-type EGFR, Y-shaped inhibitors reduce systemic toxicity.[33,34]

EAI001, EAI045, JBJ-04-125-02, and TREA-0236 (Fig. 1) are fourth-generation bis-amide-based EGFR inhibitors with Y-shaped structures. They are potent non-ATP competitive inhibitors of mutant C797S and T790M EGFR. A closer examination of these compounds' design approaches (Y configuration strategy) and typical anticancer efficacy yielded important insights into the advancement of more potent EGFR inhibitors against T790M and C797S mutations.[35,36] Although EGFR inhibitors that target the C797S mutation are being developed, small-molecule EGFR inhibitors with new motifs and enhanced drug-like qualities are still needed.

miRNAs are a subclass of short non-coding RNA molecules that range in length from 19 to 23 nucleotides.[37] miRNAs control gene expression by directly binding to mRNAs' matching sites, which causes the target mRNAs to degrade quickly.[38]

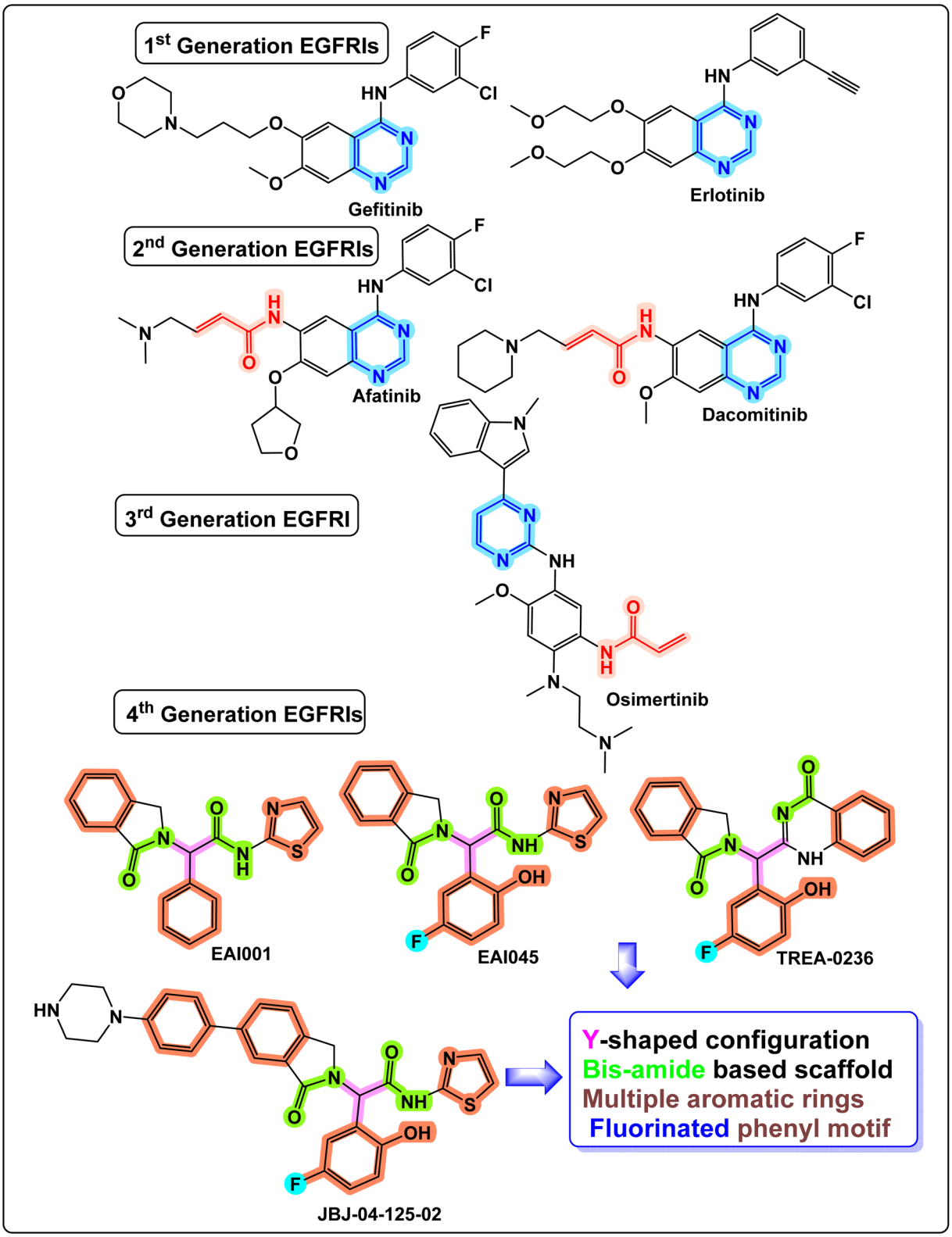

Fig. 1 The four generations of EGFR inhibitors.

miRNAs affect numerous important cellular processes, including cell proliferation, apoptosis, angiogenesis, invasion, and migration. They also have a role in several biological processes, including organism growth, immunological control, and carcinogenesis.[39,40] miRNAs have received increased attention due to their numerous applications as regulatory molecules

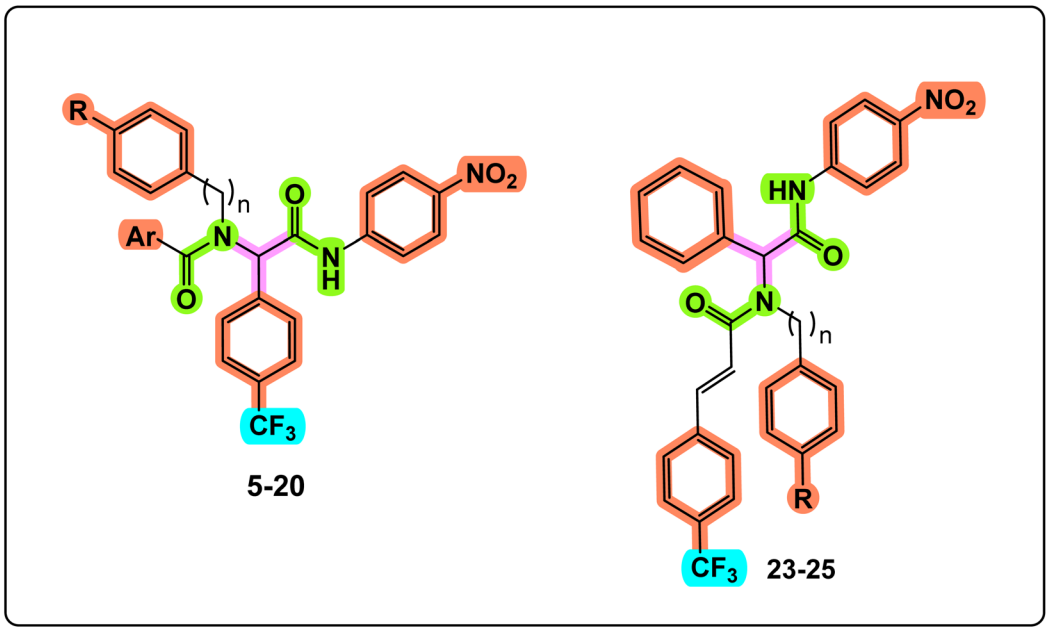

Fig. 2 The design of targeted Ugi adducts as fourth-generation EGFR inhibitors.

in numerous signaling transductions, including the EGFR signaling pathway acting as oncomirs or tumor suppressors in several cancer types.[41] Recently, miRNAs have been associated with lung cancer cells' resistance to anti-EGFR drugs, suggesting that miRNAs could be helpful as new targets or promising predictive biomarkers for anti-EGFR treatment.[41]

Due to their simple synthesis, ease of structural diversification, chemical stability, and effectiveness as potential anticancer candidates,[42–50] exerting their anticancer efficacy *via* different mechanisms such as tyrosine kinases inhibition, activation of caspases, and apoptosis induction, the Ugi scaffolds are privileged structures that earned a great interest in medicinal chemistry. The amide motif as a backbone scaffold is also important since it is the most widely used in bioactive compounds, including peptidomimetics.[47]

Inspired by all these findings, we have designed and synthesized a series of novel Ugi adducts (Fig. 2) with a Y-shaped configuration imitating the thematic feature of fourth-generation EGFR inhibitors (bis-amide-based scaffold featuring multiple aromatic rings with a fluorinated phenyl motif). The synthesized Ugi adducts were simply prepared *via* a one-step Ugi four-component reaction. They are based on bis-amides and incorporate multiple aromatic or heteroaromatic rings. Some of these aromatic rings feature different arrays of electron-donating and electron-withdrawing substituents that influence the electrical environment and spatial arrangement of the scaffolds. This diversity of substitutions may impact the anticancer potential of the target Ugi adducts and enable us to conduct a study of the structure–activity relationship. Within the framework of imitation design, we have incorporated the trifluoromethyl (CF_3) group on one phenyl ring of the targeted Ugi adducts. The inclusion of CF_3 moiety in the designed drug candidates often aimed to enhance their potencies.[51–53] Some of the aromatic rings are incorporated in the Ugi scaffold *via* variable linkers that differ in length, and some of these linkers were selected to be shared as H-bond acceptors and/or donors in the EGFR active site.

The synthesized Ugi adducts were assessed for their cytotoxic efficacy against A549 non-small cell lung cancer and MDA-MB-231 human breast carcinoma cell lines. Their selectivity was assessed using normal human lung epithelial cells (BEAS-2B) to investigate the synthesized compounds' safety for normal cells. The concentration that results in 50% inhibition of cell viability (IC_{50}) values of all synthesized Ugi adducts was calculated. The most potent Ugi adduct was subjected to further enzymatic and mechanistic investigations, such as *in vitro* EGFR inhibition assay against human wild and human triple (L858R/T790M/C797S) mutant types and caspase 3/9 activation to assess its apoptotic induction potential. The impact of the most prominent Ugi adduct on regulating markers related to the proliferation, invasion, and migration of human cancer cells (c-Myc, CD44, CD133, VEGF, and TGF) was investigated. Its impact on the expression of miRNA-132 and miRNA-200c was also evaluated.

2. Results and discussion

2.1. Chemistry

Ugi reaction is a versatile and highly efficient synthetic strategy for synthesizing highly functionalized di-peptide-like products with structural diversity and high efficiency.[54,55] Moreover, introducing different functionalized or substituents on these active peptidomimetic products may enhance their affinity and bioavailability as effective pharmaceutical agents and their selectivity and potency towards specific biological targets. Among these substituents is the trifluoromethyl (CF_3) group, which is one of the most lipophilic functional groups.[56–58] The

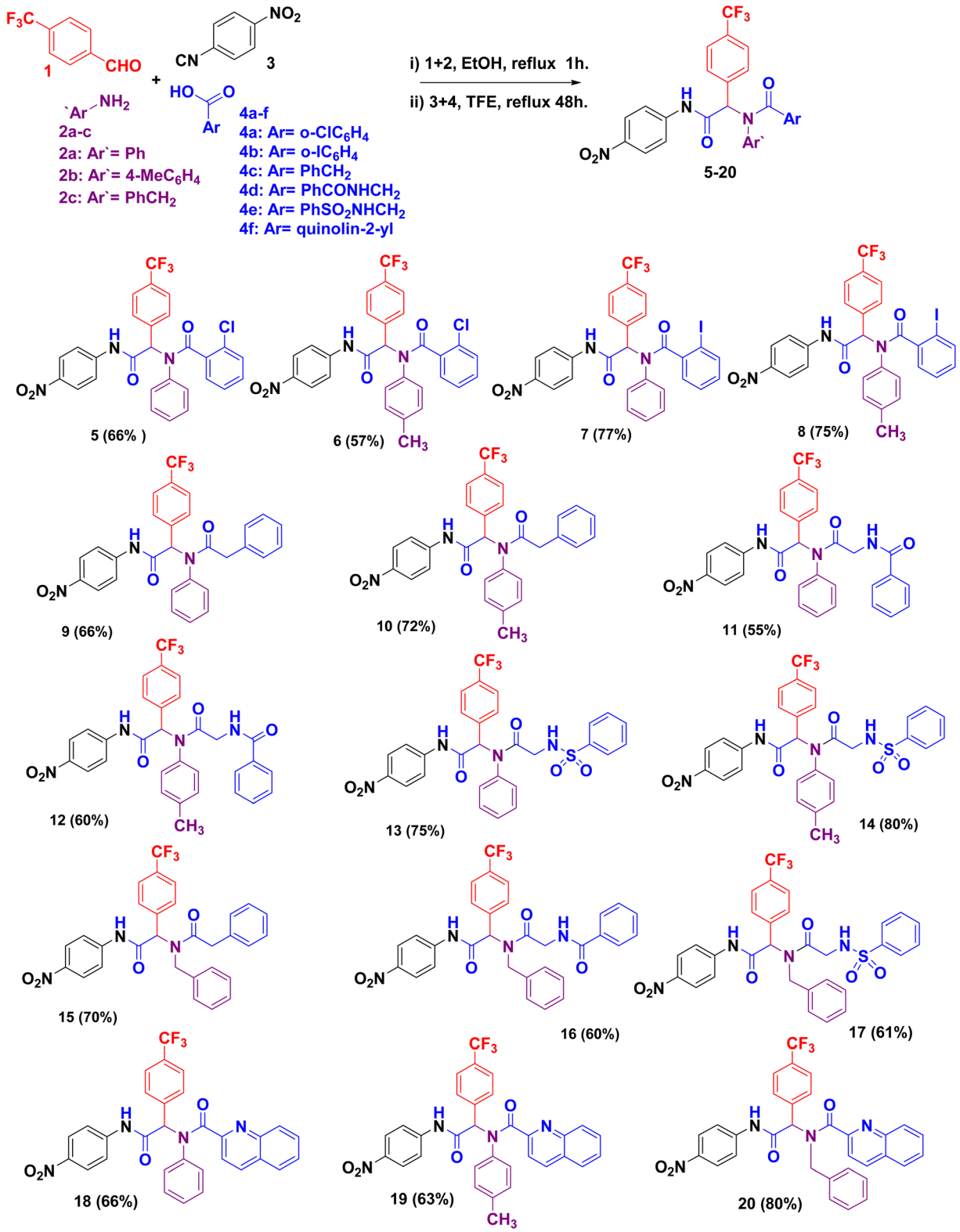

Scheme 1 Synthesis of fluorinated Ugi products 5–20.

inclusion of CF_3 moiety in the molecules often aimed to improve metabolic stability and hydrophobicity in drug development.[59] Moreover, combining aromatic trifluoromethyl moieties with other organic compounds will enhance their potency as biologically active derivatives.[51–53,60–69] Accordingly, we focused here on constructing diverse functionalized Ugi products with trifluoromethyl moiety for their evaluation as anticancer products.

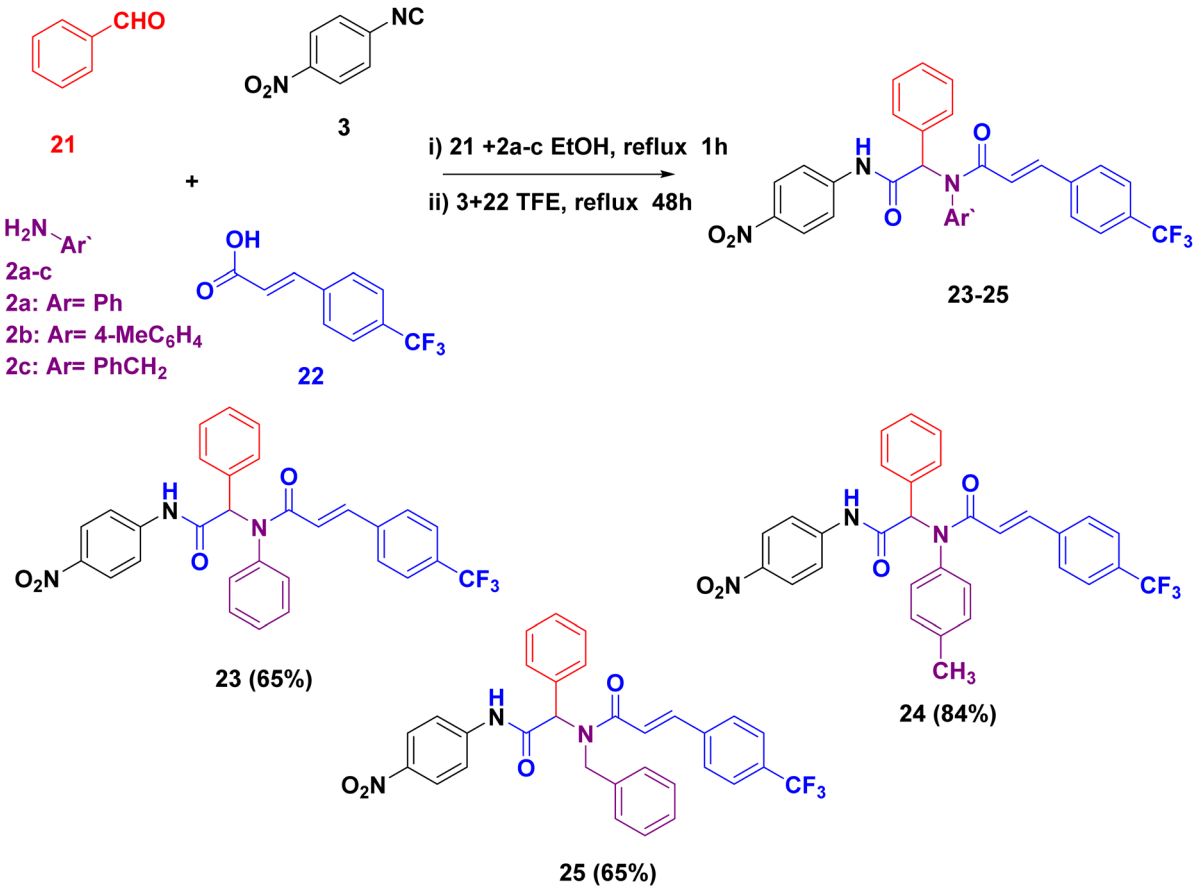

Scheme 2 Synthesis of Ugi products based fluorinated cinnamide **23–25**.

The synthesis of the target Ugi products having the desired lipophilic trifluoromethyl group, which we expect to enhance the bioavailability of the synthesized products, has been attempted through two pathways of Ugi multi-component reaction (Schemes 1 and 2).

This can be either through the coupling of *p*-trifluoromethyl benzaldehyde, carboxylic acid derivatives, or benzaldehyde and *p*-trifluoromethyl cinnamic acid instead. Thus, the coupling reaction of *p*-trifluoromethyl benzaldehyde **1** and aniline derivative **2a–b** or benzylamine **2c** was carried out in ethanol under reflux for 1 h followed by the addition isonitrile **3** and the appropriate carboxylic acids **4a–f** in 2,2,2-trifluoroethanol (TFE) afforded the Ugi products **5–20** in 55–80% yield within 48 under reflux (Scheme 1). Alternatively, compounds **23–25** were obtained in 65–84% yield under the same reaction conditions using benzaldehyde and *p*-trifluoromethyl cinnamic acid (Scheme 2) where the Ugi reaction conditions were optimized as reported previously.[49]

Structure elucidation of the synthesized compounds was confirmed from their spectral analyses. The NMR spectrum pattern of compounds **5–19**, and **23–25** differed according to the carboxylate moiety introduced as well as the amine used. The purity of the most active compound **5** was confirmed by HRMS, which reported that the exact mass experimentally aligned with the theoretically calculated mass. However, characteristic functional signals were common. Thus, the trifluoromethyl group was assigned at δ_C 125.5–125.7 ppm in the ^{13}C NMR spectra. Two amidic carbon (CON) signals were observed at δ_C 165.4–169.7 and 169.1–172.9 ppm, whereas the respective NH proton (CON**H**) resonated at δ_H 10.93–11.14 ppm as a D_2O exchangeable singlet. Moreover, the methine proton NC**H**CO resonated at δ_H 6.24–6.75 ppm, which correlated with its carbon at δ_C 62.9–65.6 ppm for above mentioned compounds. The result and discussion of NMR and IR results of the other Ugi product were reported in the ESI file.†

2.2. Biological evaluation

2.2.1. Cytotoxicity screening. All the newly synthesized Ugi adducts were investigated for potential cytotoxic activities on normal human lung epithelial cells (BEAS-2B), breast cancer (MDA-MB-231), and non-small cell lung cancer (NSCLC, A549) cell lines compared to 5-fluorouracil (5-FU) and cisplatin adopting MTT assay[70] (Table 1). The highest potencies against MDA-MB-231 cells were exhibited by Ugi adducts **5**, **7**, **8**, **16**, **18**, **23**, and **24** with IC_{50} values in the range of 10.1 to 30.3 μM. Interestingly, the Ugi adduct **5** (IC_{50} = 10.1 μM) was the most prominent against the breast cancer cell line among the tested Ugi adducts; it was 1.42 and 1.20-fold more potent than 5-FU and cisplatin with IC_{50} values of 14.4 and 12.2 μM, respectively. Compounds **7**, **8**, **16**, **18**, and **24** exhibited cytotoxicity

Table 1 Cytotoxicity and selectivity index (SI) values of the tested Ugi adducts

	BEAS-2B	MDA-MB-231		A549	
Compound no.	IC_{50}[a] (μM)	IC_{50}[a] (μM)	SI	IC_{50}[a] (μM)	SI
5	70.4 ± 5.1	10.1 ± 0.6	7	6.2 ± 0.3	11.7
6	50.1 ± 3.6	54.2 ± 4.7	0.9	39.9 ± 2.7	1.3
7	75.6 ± 5.8	28.2 ± 1.4	2.7	20.6 ± 1.5	3.8
8	62.2 ± 4.2	27.1 ± 1.8	2.3	20.5 ± 1.1	3.1
9	71.6 ± 5.7	70.6 ± 6.1	1	46.4 ± 2.8	1.5
10	83.3 ± 6.8	84.4 ± 6.9	1	71.5 ± 6.8	1.2
11	82.1 ± 7.3	60.2 ± 4.9	1.4	53.9 ± 4.4	1.5
12	98.2 ± 8.1	65.3 ± 4.7	1.5	73.1 ± 6.6	1.3
13	98.5 ± 7.4	73.9 ± 5.3	1.3	64.1 ± 5.9	1.5
14	84.7 ± 6.9	74.8 ± 6.1	1.1	55.3 ± 4.2	1.5
15	69.4 ± 4.7	65.7 ± 5.4	1.1	61.1 ± 4.5	1.1
16	63.8 ± 4.8	27.3 ± 1.5	2.3	22.4 ± 0.8	2.9
17	50.2 ± 3.4	57.0 ± 4.8	0.9	40.8 ± 2.8	1.3
18	55.7 ± 3.5	25.1 ± 1.9	2.2	20.1 ± 1.4	2.8
19	50.1 ± 3.3	73.1 ± 5.7	0.7	46.2 ± 4.1	1.1
20	40.7 ± 2.8	40.2 ± 3.1	1	33.3 ± 2.1	1.2
23	30.9 ± 2.3	30.3 ± 2.4	1	26.1 ± 2.1	1.2
24	54.2 ± 4.1	22.1 ± 1.6	2.5	20.4 ± 1.7	2.7
25	129.1 ± 8.7	95.4 ± 8.1	1.4	90.2 ± 8.5	1.4
Cisplatin	5.7 ± 0.3	12.2 ± 0.8	0.47	10.1 ± 0.7	0.56
5-FU	7.2 ± 0.5	14.4 ± 0.9	0.5	11.3 ± 1.1	0.64

[a] All values are expressed as mean ± SEM.

comparable to 5-FU. Anti-proliferative screening results against A549 cells showed that compounds **5**, **7**, **8**, **16**, **18**, **23**, and **24** with IC_{50} values in the range of 6.2 to 26.1 μM demonstrated significant cytotoxicity comparable to that of 5-FU and cisplatin with IC_{50} values of 11.3 and 10.1 μM, respectively. The Ugi adduct **5** (IC_{50} = 6.2 μM) stood up as the most potent compound against non-small cell lung cancer cell line among the tested Ugi adducts; it was 1.82 and 1.62-fold more potent than 5-FU and cisplatin, respectively. Other synthesized Ugi adducts showed lower anti-proliferative potential against both cancer cell lines. Potency is a crucial factor, but a true assessment of the screening compounds depends on how safe they are for normal cells and how selective they are for malignant cells. According to an *in vitro* cytotoxicity assay against normal human lung epithelial cells (BEAS-2B) (Table 1). The screened Ugi adducts with IC_{50} values in the range of 30.9 to 129.1 μM were less toxic than 5-FU and cisplatin, with IC_{50} values of 7.2 and 5.7 μM, respectively. All Ugi adducts were assessed based on their selectivity index values (SI) (Table 1). The selectivity index shows that cancer cells are the target of the cytotoxic action, not healthy cells. It can be defined as the ratio of a compound's inhibitory concentration (IC_{50}) against normal cells divided against cancer cells. All compounds with SI values in the range of 0.7 to 11.7 were more selective against MDA-MB-231 and A549 cells than the reference drugs, 5-FU and cisplatin. Interestingly, compounds **5**, **7**, **8**, **16**, **18**, and **24** showed the highest SI values and demonstrated exceptionally high safety profiles. Compound **5** was the most potent Ugi adduct against the two screened cancer cell lines compared to all screened compounds as well as 5-FU and cisplatin. Additionally, it demonstrated the most prominent selectivity against MDA-MB-231 and A549 cells (SI = 7 and 11.7, respectively), which was subjected to further enzymatic and mechanistic studies.

2.2.1.1. Structure–activity relationship. A promising anti-proliferative potential demonstrated by the bis-amide Ugi scaffold design is reflected in the overall cytotoxic activity pattern. An interesting phenomenon is that the most prominent Ugi adducts (**5**, **7**, **8**, **16**, **18**, **23**, and **24**) demonstrated significant cytotoxicity against both non-small cell lung cancer (NSCLC, A549) and breast cancer (MDA-MB-231) cell lines at the same time demonstrated exceptionally the highest safety profiles. The activity profile demonstrated a higher potency of the synthesized Ugi adducts against non-NSCLC, A549 cell line than MDA-MB-231 cell line. The combinatorial diversity of Ugi components determined the anticancer profile (Fig. 3). Concerning modifications of Ugi aldehyde component, results showed that the derivatives derived from *p*-trifluoromethyl benzaldehyde (**5**, **7**, **8**, **16**, and **18**) endowed better anti-proliferative potential than those derived from benzaldehyde (**23** and **24**), reflecting the positive impact on the cytotoxicity of closer proximity of the trifluoromethylphenyl moiety from the bis-amide Ugi scaffold. Further combinatorial modifications are based on diversifying carboxylic acid derivatives. The incorporation of halogen (Cl or I) in the Ugi adducts greatly improved the antitumor activities (compounds **5**, **7**, and **8** derived from halogenated carboxylic acids). Further analysis of these compounds revealed that shifting of iodo to chloro group introduced the most active Ugi adduct **5** in the current study. Increasing the length of the linker connecting the aromatic motif of the carboxylic acid component of the Ugi adduct in compounds **9–15** endowed a remarkable reduction in anti-proliferative potency. Ugi bis-amides derived from aniline or *p*-toluidine (**5**, **7**, **8**, **18**, **23**, and **24**) were more potent anticancer agents than adducts derived from benzylamine.

2.2.2. $EGFR^{WT}$ kinase inhibition assay. The most potent Ugi adduct **5** was exposed to an additional *in vitro* $EGFR^{WT}$ inhibition assay using six distinct concentrations (0.001, 0.01, 0.1, 1, and 10 μM). The percentage of *in vitro* inhibition of EGFR-TK at the different concentrations was measured, and a dose–response curve was constructed for the tested compound and utilized for calculating the IC_{50} value. Results were illustrated as the IC_{50} value of compound **5** compared to erlotinib as a standard drug (Table 2). Results showed that compound **5** showed excellent nanomolar potency (IC_{50} = 2.1 nM), which was comparable to that of the reference standard erlotinib (IC_{50} = 1.3 nM).

2.2.3. $EGFR^{T790M/C797S/L858R}$ kinase inhibition assay. Compound **5** was investigated for its ability to inhibit the triple mutant $EGFR^{L858R/T790M/C797S}$ enzyme at six distinct concentrations (0.001, 0.01, 0.1, 1, and 10 μM). The percentage of mutant $EGFR^{L858R/T790M/C797S}$ inhibition *in vitro* at various concentrations was determined, and a dose–response curve was created for the tested Ugi adduct, which was then used to determine the IC_{50} value. The IC_{50} value of compound **5** compared to osimertinib (AZD9291) as a reference standard was used to demonstrate the results (Table 2). Results showed that compound **5** showed excellent sub-micromolar potency (IC_{50} =

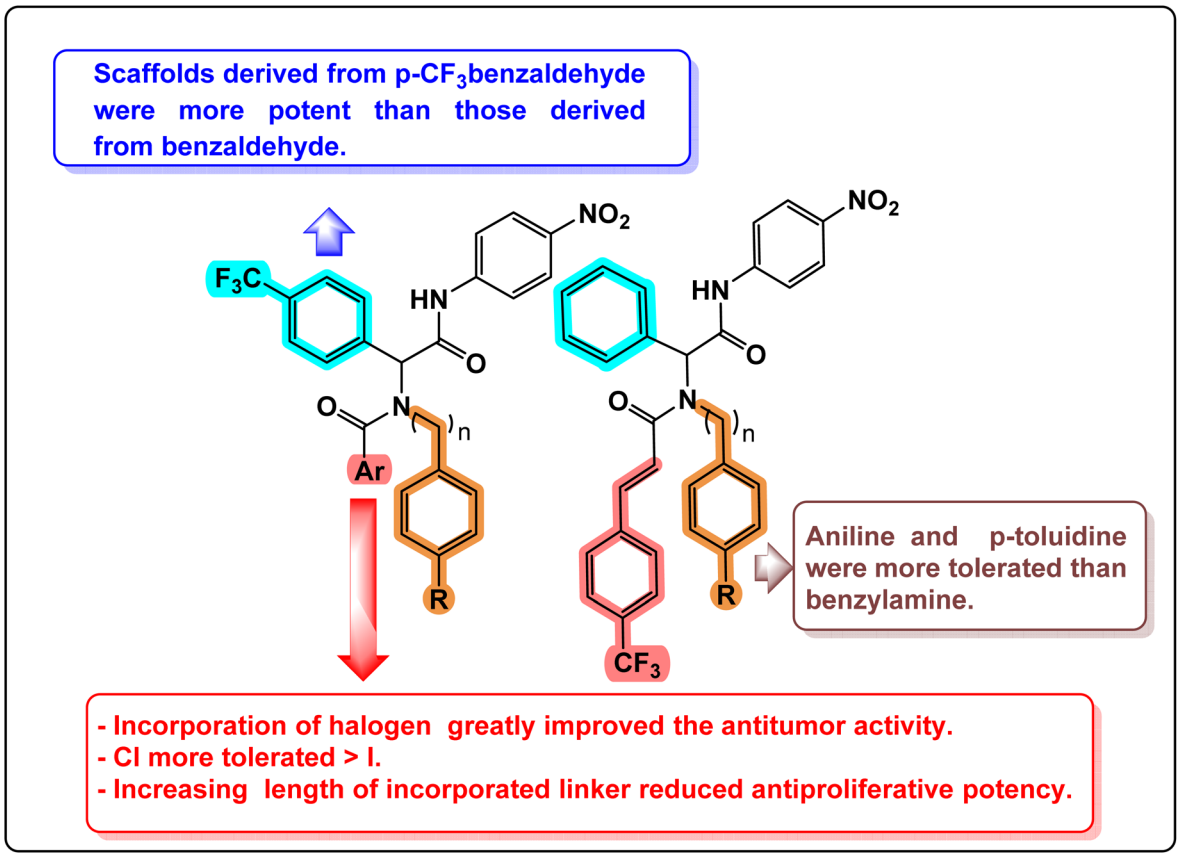

Fig. 3 The structure–activity relationship of the synthesized Ugi adducts.

Table 2 IC_{50} values against $EGFR^{WT}$ and $EGFR^{L858R/T790M/C797}$ enzymes

Enzyme	5	Erlotinib	Osimertinib
	Compound IC_{50}[a] (nM)		
$EGFR^{WT}$	2.1 ± 0.01	1.3 ± 0.05	ND
	Compound IC_{50}[a] (μM)		
$EGFR^{L858R/T790M/C797S}$	0.19 ± 0.05	ND	0.1 ± 0.01

[a] All values are expressed as mean ± SD. ND: not determined.

0.19 μM), which was equipotent to the standard osimertinib (IC_{50} = 0.1 μM).

2.2.4. Effect of compound 5 on the expression of c-Myc, CD-44, CD-133, VEGF, and TGF markers. To investigate the effect of the Ugi adduct **5** in regulating the cell proliferation, migration, and invasion potentialities of MDA-MB-231 and A549 human cancer cells. The expression of cancer initiation, angiogenic, and metastatic markers (c-Myc, CD-44, CD-133, VEGF, and TGF) were measured in both MDA-MB-231 and A549 cells after compound **5** exposure. These markers are highly amplified in many human cancers. They regulate different stages of cancer development, including initiation, progression, and advancement (invasion and metastasis).[71–75] In MDA-MB-231 human cancer cells, compound **5** induced a reduction in the expression of c-Myc, CD-44, CD-133, VEGF, and TGF markers to 0.36, 0.5, 0.7, 0.5, and 0.4-folds, respectively, compared to untreated control (Fig. 4). Regarding A549 cells, the exposure to compound **5** showed 0.41, 0.64, 0.58, 0.71, and 0.69-fold reduction in the expression of c-Myc, CD-44, CD-133, VEGF, and TGF markers in comparison to untreated control (Fig. 4).

2.2.5. Effect of compound 5 on the expression of miRNA-132 and miRNA-200c. Overexpression of miRNA-132 and miRNA-200c prevents cancer cells from migrating and invading other cells, indicating that these two microRNAs are suppressors of cancer cell metastasis.[76,77] The expression of miRNA-132 and miRNA-200c was measured in MDA-MB 231 and A549 human cancer cells after treatment with the Ugi adduct **5** and compared to untreated cancer cells. The results disclosed that compound **5** markedly elevated miRNA-132 and miRNA-200c expressions in the MDA-MB-231 cell line by 3.8 and 3.1-fold changes compared to control, while in A549 cells, **5** demonstrated enhancement of miRNA-132 and miRNA-200c expression by 2.4 and 1.9-fold changes compared to that of control (Fig. 5).

2.2.6. The effect of compound 5 on levels of the apoptotic markers caspases 3 and 9. The hallmarks of the apoptotic degradation phase, such as DNA fragmentation, cell shrinkage, and membrane blebbing, are mediated by effector caspases. Apoptosis is initiated by the activation of caspase-3 and caspase-

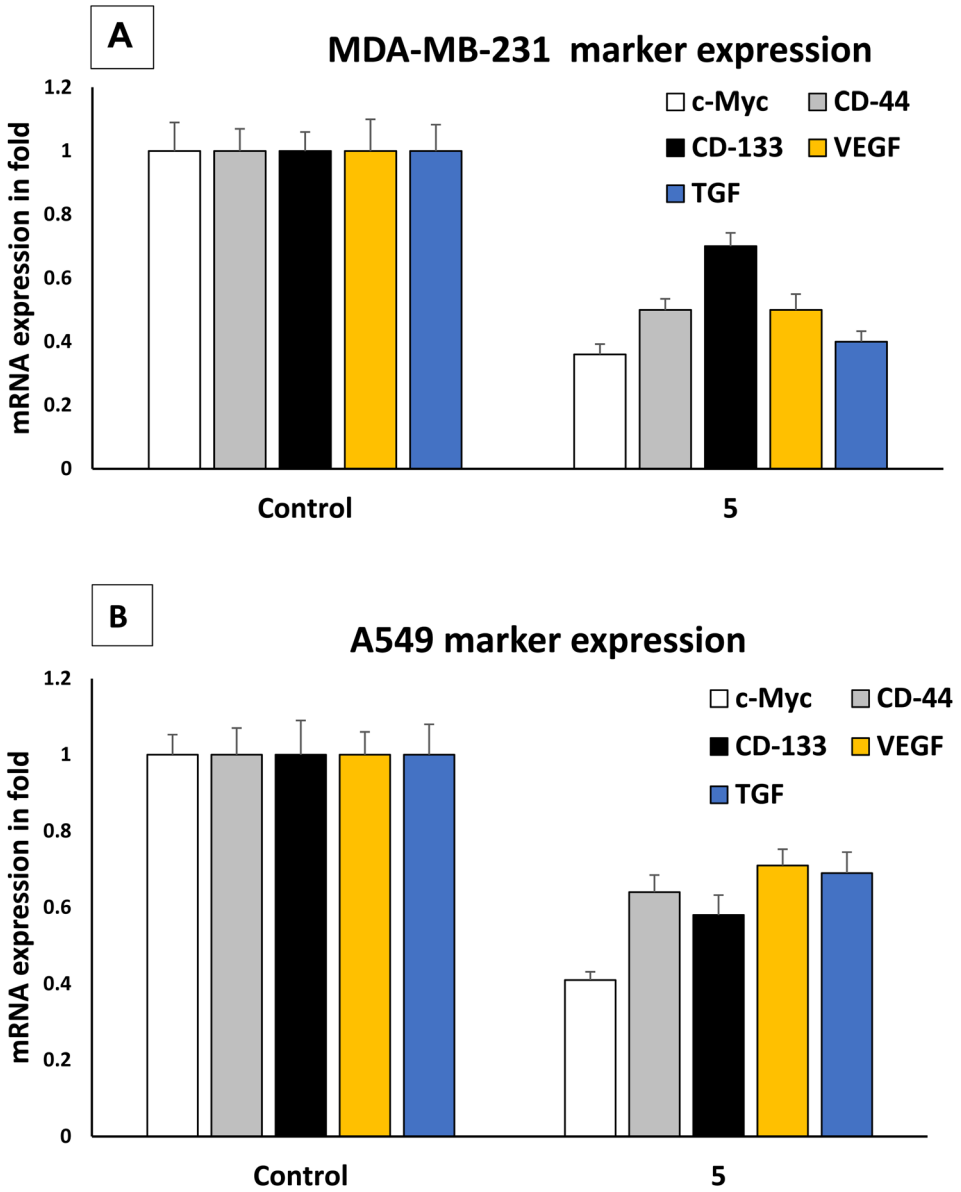

Fig. 4 (A) Effect of Ugi adduct **5** on the expression of c-Myc, CD-44, CD-133, VEGF, and TGF in MDA-MB 231 cells. (B) Effect of Ugi adduct **5** on the expression of c-Myc, CD-44, CD-133, VEGF, and TGF in A549 cells.

9, especially caspase-3, an effector caspase that plays a crucial part in the process through the activation of certain enzymes that cause fragmentation of DNA.[78] By determining the percentage of caspase 3/9 activation in the human cancer cell line A549, the mechanistic study of apoptotic enhancement by the promising adduct **5** was assessed by applying the studied compound to the cancer cells at its IC_{50} concentration. The results revealed that compound **5** exhibited upregulation of caspase-3 and caspase-9 in the treated lung cancer cell line by 1.8 and 2.3 folds, respectively, compared to the untreated control (Fig. 6).

2.2.7. Molecular docking studies. The molecular docking study aimed to investigate the dual potency of compound **5** against both wild-type and mutant EGFR and to explore which enantiomer is primarily responsible for the observed biological activity. Molecular docking of both enantiomers was performed, and the results were used to predict their binding interactions with $EGFR^{L858R/T790M/C797S}$ (PDB ID: 6LUB)[79] and the wild-type $EGFR^{WT}$ (PDB ID: 1M17).[80] In the wild-type EGFR, the docking results (Fig. 7) showed that the *R*-enantiomer of compound **5** formed three hydrogen bonds with Met742 (3.42 Å), Asp831 (3.45 Å), and Cys773 (2.89 Å), one pi–hydrogen interaction with Gly695, and one pi–cation interaction with Lys721, with a binding energy score of −7.16 kcal mol^{-1}. The interaction of the *R*-enantiomer of compound **5** with mutant EGFR (Fig. 8) involved five hydrogen bond interactions with Asp855 (3.18 Å), Met790 (4.23 Å and 3.43 Å), Lys745 (2.93 Å) and Gly719 (3.42 Å) in addition to two pi–hydrogen interactions with Arg841 and Leu718 (the binding energy score = −7.57 kcal mol^{-1} $kcal^{-1}$ mol^{-1}). The *S*-enantiomer showed a comparable binding energy

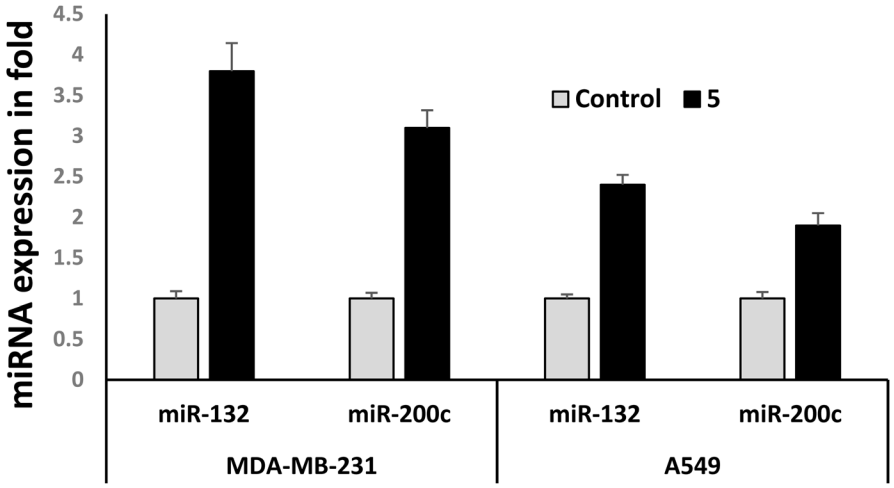

Fig. 5 Effect of Ugi adduct **5** on the expression of miRNA-132 and miRNA-200c in MDA-MB 231 and A549 cells.

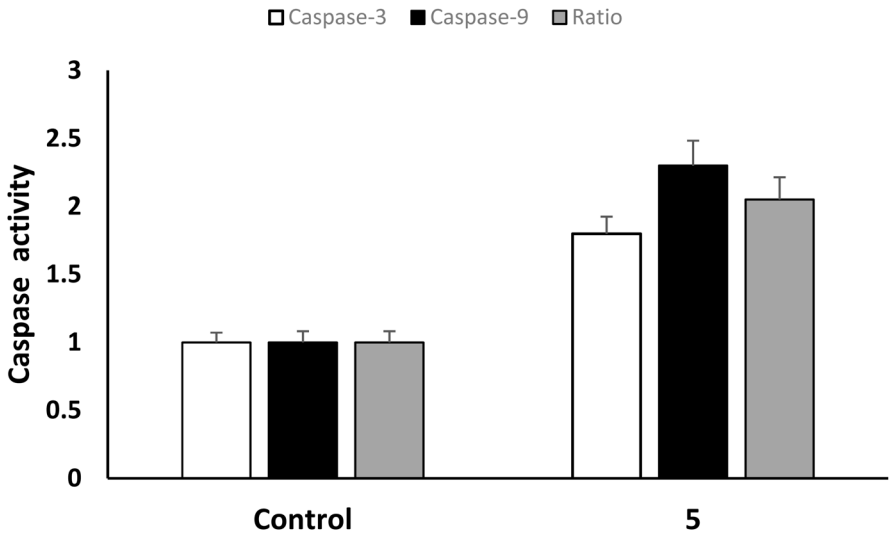

Fig. 6 Effect of Ugi adduct **5** on the levels of caspase-3 and caspase-9 in A549 cells.

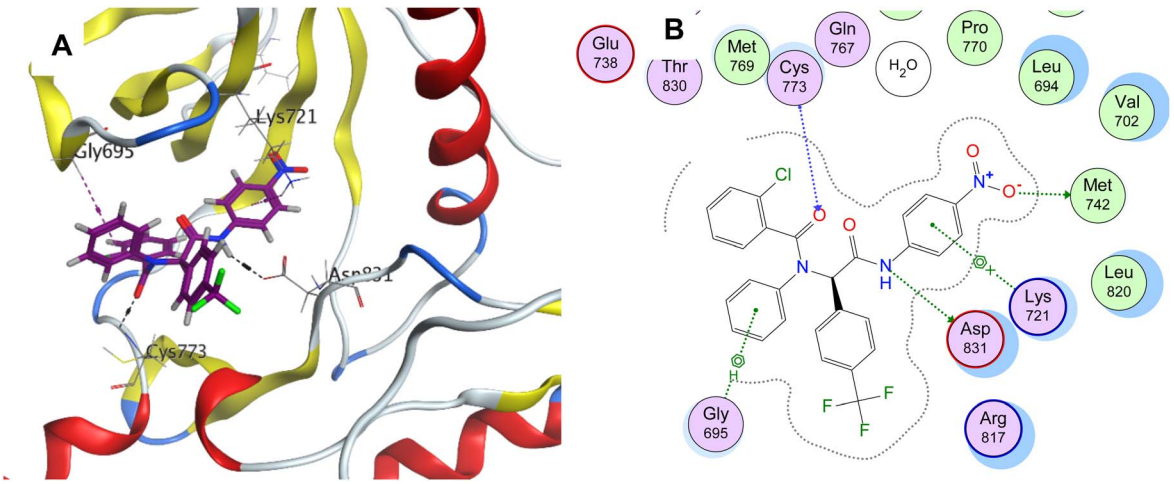

Fig. 7 (A) 3D representation and (B) 2D representation of *R*-enantiomer of compound **5** binding with the binding pocket of the wild-type EGFR^{WT} enzyme (PDB ID: 1M17).

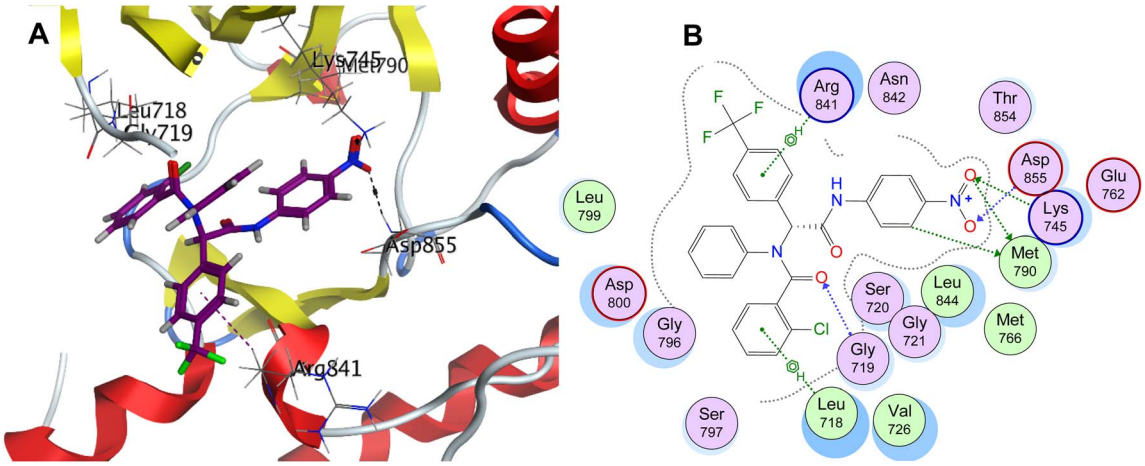

Fig. 8 (A) 3D representation and (B) 2D representation of *R*-enantiomer of compound **5** binding with the binding pocket of the mutant $EGFR^{L858R/T790M/C797S}$ (PDB ID: 6LUB).

score but formed fewer interactions with both $EGFR^{WT}$ and $EGFR^{L858R/T790M/C797S}$ (ESI†), suggesting that the *R*-enantiomer may primarily contribute to the biological activity. Overall, the molecular docking studies of Ugi adduct **5** demonstrated favorable binding within the active sites of both $EGFR^{WT}$ and $EGFR^{L858R/T790M/C797S}$, supporting its potential to inhibit both enzymes dually.

3. Conclusion

The current study reports the synthesis of novel Ugi adducts as potential anti-proliferative agents *via* a one-step Ugi four-component reaction. Utilizing NMR and elemental analysis, all synthesized adducts were verified. The anti-proliferative potential of the synthesized Ugi adducts against human breast cancer MDA-MB-231 and non-small cell lung carcinoma A549 was evaluated by adopting the MTT assay. The BEAS-2B normal human lung epithelial cells were used to evaluate their selectivity. Concerning cytotoxic activity and selectivity, the Ugi adduct **5** emerged as the study hit. Against the MDA-MB-231 cell line, it was 1.42 and 1.20 times more potent than 5-FU and cisplatin, respectively. When applied to the A549 cell line, it was 1.82 and 1.62 times more potent than 5-FU and cisplatin. Additionally, compound **5** demonstrated the most prominent selectivity against MDA-MB-231 and A549 cells (SI = 7 and 11.7, respectively). Excellent sub-micromolar potency (IC_{50} = 0.19 μM) was demonstrated by the Ugi adduct **5** against the human mutant $EGFR^{T790M/C797S/L858R}$ enzyme equipotent with that of osimertinib (IC_{50} = 0.1 μM). It demonstrated a promising IC_{50} value of 2.1 nM against the $EGFR^{WT}$ enzyme, comparable to erlotinib (IC_{50} = 1.3 nM). In comparison to the untreated control, the Ugi adduct **5** caused a decrease in the expression of the cancer initiation, angiogenic, and metastatic markers (c-Myc, CD-44, CD-133, VEGF, and TGF) to 0.36, 0.5, 0.7, 0.5, and 0.4-folds, respectively in MDA-MB-231 cells. Regarding A549 cells, the exposure to compound **5** showed a 0.41, 0.64, 0.58, 0.71, and 0.69-fold reduction in the expression of c-Myc, CD-44, CD-133, VEGF, and TGF markers in comparison to untreated control. In the MDA-MB-231 cell line, compound **5** significantly increased the expression of miRNA-132 and miRNA-200c by 3.8 and 3.1-fold, respectively. In A549 cells, compound **5** showed improvements in miRNA-132 and miRNA-200c expression by 2.4 and 1.9-fold relative to the control. Through caspase 3/9 activation (1.8- and 2.3-folds), it promoted apoptosis in the A549 cell line. The molecular docking interpretations of the most potent Ugi adduct **5** in $EGFR^{L858R/T790M/C797S}$ (PDB ID: 6LUB) and the wild-type $EGFR^{WT}$ (PDB ID: 1M17) enzymes are aligned with and explain its potential to dually inhibit $EGFR^{L858R/T790M/C797S}$ and $EGFR^{WT}$ tyrosine kinases. It can be concluded that the synthesized Ugi adduct **5** represents a promising novel lead scaffold of $EGFR^{T790M/C797S/L858R}$ inhibitors and a possible anti-proliferative drug candidate that warrants additional investigation.

4. Experimental

4.1. Chemistry

4.1.1. The general method for the synthesis of Ugi adducts (5–20). A mixture of 4-(trifluoromethyl)benzaldehyde **1** (0.67 mmol) and aniline derivatives **2a–b** (0.67 mmol), or benzylamine **2c** (0.67 mmol) in ethanol (2 ml) was stirred under reflux for 1 h then, the appropriate carboxylic acids **4a–f** (0.67 mmol), isonitrile **3** (0.67 mmol) and trifluoroethanol (2 ml) were added with stirring. The reaction mixture was heated under reflux while stirring for a further 48 h. The crude obtained was filtered off, washed with ethanol, dried, and crystallized from ethanol.

4.1.1.1. 2-Chloro-N-(2-((4-nitrophenyl)amino)-2-oxo-1-(4-(trifluoromethyl)phenyl)ethyl)-N-phenylbenzamide (5). Off-white powder (66% yield), m.p = 237–239 °C; R_f = 0.628 (EtOAc : *n*-hexane, 1 : 2); IR (KBr, cm^{-1}): 3296 (N–H), 1711, 1629 (OCN); ^1H NMR (500 MHz, DMSO-d_6) δ_H: 11.10 (s, 1H, D_2O exchangeable, N–**H**), 8.23 (d, 2H, J = 9.0 Hz, Ar–**H**), 7.88 (d, 2H, J = 9.0 Hz, Ar–**H**), 7.55 (d, 2H, J = 8.5 Hz, Ar–**H**), 7.42 (d, 2H, J = 7.5 Hz, Ar–**H**), 7.29–7.23 (m, 2H, Ar–**H**), 7.15–7.09 (m, 4H, Ar–**H**), 6.95–6.89 (m, 3H, Ar–**H**), 6.47 (s, 1H, NC**H**CO); ^{13}C NMR (125 MHz, DMSO-d_6) δ_C: 169.1, 168.1 (CON), 145.4, 143.0, 138.7, 138.5, 136.5, 131.7

(C–Cl), 131.1, 130.7, 129.8, 129.6, 129.5, 129.3, 129.2, 128.6, 128.5, 127.1, 125.7, 119.6 (Ar–C), 125.5 (**C**F_3), 64.7 (N**C**HCO); anal. calc. for $C_{28}H_{19}ClF_3N_3O_4$ (553.10162): C, 60.71; H, 3.46; N, 7.59. Found; C, 60.97; H, 3.61; N, 7.35. HRMS (ESI$^+$) m/z $[M+H]^+$ cald for $C_{28}H_{20}ClF_3N_3O_4^+$: 554.10944, found: 554.10753.

*4.1.1.2. 2-Chloro-N-(2-((4-nitrophenyl)amino)-2-oxo-1-(4-(trifluoromethyl)phenyl)-ethyl)-N-(p-tolyl)benzamide (**6**).* White powder (57% yield), m.p = 255–257 °C; R_f = 0.628 (EtOAc : *n*-hexane, 1 : 2); IR (KBr, cm^{-1}): 3369 (N–H), 1704, 1635 (OCN); ^{1}HNMR (500 MHz, DMSO-d_6) δ_H:11.07 (s, 1H, D_2O exchangeable, N–**H**), 8.22 (d, 2H, J = 9.5 Hz, Ar–**H**), 7.87 (d, 2H, J = 9.0 Hz, Ar–**H**), 7.57 (d, 2H, J = 8.5 Hz, Ar–**H**), 7.41 (d, 2H, J = 8.5 Hz, Ar–**H**), 7.28–7.23 (m, 2H, Ar–**H**), 7.16–7.10 (m, 2H, Ar–**H**), 7.03 (bs, 2H, Ar–**H**), 6.75 (d, 2H, J = 8.0 Hz, Ar–**H**), 6.45 (s, 1H, NC**H**CO), 1.97 (s, 3H, **C**H_3); ^{13}C NMR (125 MHz, DMSO-d_6) δ_C: 169.1, 168.4 (CON), 145.3, 143.0, 138.6, 137.7, 136.6, 136.1, 131.7 (C–Cl), 130.8, 130.7, 130.7, 129.7, 129.6, 129.4, 129.3, 129.2, 129.1, 127.1, 125.7, 125.6, 119.6 (Ar–C), 125.5 (**C**F_3), 64.7 (N**C**HCO), 20.8 (**C**H_3); anal. calc. for: $C_{29}H_{21}ClF_3N_3O_4$ (567.95): C, 61.33; H, 3.73; N, 7.40. Found; C, 61.54; H, 3.82; N, 7.23.

*4.1.1.3. 2-Iodo-N-(2-((4-nitrophenyl)amino)-2-oxo-1-(4-(trifluoromethyl)phenyl)ethyl)-N-phenyl-benzamide (**7**).* Off-white powder (77% yield), m.p = 240–243 °C; R_f = 0.628 (EtOAc : *n*-hexane, 1 : 2); IR (KBr, cm^{-1}): 3299 (N–H),1712, 1625 (OCN); ^{1}H NMR (500 MHz, DMSO-d_6) δ_H: 11.12 (bs, 1H, D_2O exchangeable, N–**H**), 8.22 (d, 2H, J = 9.5 Hz, Ar–**H**), 7.87 (d, 2H, J = 9.0 Hz, Ar–**H**), 7.63 (d, 1H, J = 8.5 Hz, Ar–**H**), 7.56 (d, 3H, J = 8.5 Hz, Ar–**H**), 7.40 (d, 2H, J = 7.5 Hz, Ar–**H**), 7.21–7.13 (m, 3H, Ar–**H**), 6.95–6.85 (m, 4H, Ar–**H**), 6.47 (s, 1H, NC**H**CO); ^{13}C NMR (125 MHz, DMSO-d_6) δ_C: 170.4, 169.2 (CON), 143.0, 142.3, 139.1, 138.8, 138.5, 131.7, 131.2, 130.6, 129.5, 129.2, 129.0, 128.5, 128.4, 127.8, 125.8, 119.6 (Ar–C), 125.6 (**C**F_3), 94.5 (**C**–I), 64.8 (N**C**HCO); anal. calc. for $C_{28}H_{19}F_3IN_3O_4$: (645.38): C, 52.11; H, 2.97; N, 6.51. Found; C, 52.34; H, 2.74; N, 6.69.

*4.1.1.4. 2-Iodo-N-(2-((4-nitrophenyl)amino)-2-oxo-1-(4-(trifluoromethyl)phenyl)ethyl)-N-(p-tolyl)-benzamide (**8**).* Off-white powder (75% yield), m.p = 227–229 °C; R_f = 0.63 (EtOAc : *n*-hexane, 1 : 2); IR (KBr, cm^{-1}): 3222 (N–H), 1710, 1677 (OCN); ^{1}H NMR (500 MHz, DMSO-d_6) δ_H: 11.11 (bs, 1H, D_2O exchangeable, N–**H**), 8.20 (d, 2H, J = 9.0 Hz, Ar–**H**), 7.85 (d, 2H, J = 8.5 Hz, Ar–**H**), 7.63 (d, 1H, J = 7.5 Hz, Ar–**H**), 7.58 (d, 2H, J = 8.5 Hz, Ar–**H**), 7.40 (d, 2H, J = 7.5 Hz, Ar–**H**), 7.16–7.08 (m, 4H, Ar–**H**), 6.88–6.85 (m, 1H, Ar–**H**), 6.75 (d, 2H, J = 7.5 Hz, Ar–**H**), 6.44 (s, 1H, NC**H**CO), 1.99 (s, 3H, **C**H_3); ^{13}C NMR (125 MHz, DMSO-d_6) δ_C: 170.5, 169.2 (CON), 143.0, 142.4, 141.0, 139.1, 138.7, 137.7, 130.9, 130.5, 129.6, 129.5, 129.0, 128.9, 127.8, 125.7, 119.6 (Ar–C), 125.6 (**C**F_3), 94.4 (**C**–I), 64.7 (N**C**HCO), 20.9 (**C**H_3); anal. calc. for $C_{29}H_{21}F_3IN_3O_4$ (659.40); C, 52.82; H, 3.21; N, 6.37. Found; C, 52.95; H, 3.31; N, 6.48.

*4.1.1.5. 2-(N,2-Diphenylacetamido)-N-(4-nitrophenyl)-2-(4-(trifluoromethyl)phenyl)acetamide (**9**).* White powder (66% yield), m.p = 243–245 °C; R_f = 0.57 (EtOAc : *n*-hexane, 1 : 2); IR (KBr, cm^{-1}): 3331 (N–H), 1710, 1632 (OCN); ^{1}H NMR (500 MHz, DMSO-d_6) δ_H: 10.95 (s, 1H, D_2O exchangeable, N–**H**), 8.19 (d, 2H, J = 9.0 Hz, Ar–**H**), 7.82 (d, 2H, J = 9.0 Hz, Ar–**H**), 7.50 (d, 2H, J = 7.5 Hz, Ar–**H**), 7.34 (d, 2H, J = 8.5 Hz, Ar–**H**), 7.21–7.14 (m, 8H, Ar–**H**), 7.01 (d, 2H, J = 7.0 Hz, Ar–**H**), 6.27 (s, 1H, NC**H**CO), 3.36 (d, 2H, J = 2.5 Hz, COC**H**$_2$ Ph); ^{13}C NMR (125 MHz, DMSO-d_6) δ_C: 171.1, 169.6 (CON), 145.4, 142.9, 139.4, 138.9, 135.9, 131.7, 131.5, 129.7, 129.3, 128.7, 128.6, 126.9, 125.7, 125.6, 119.5 (Ar–C), 125.5 (**C**F_3), 64.5 (N**C**HCO), 41.2 (CO**C**H_2Ph); anal. calc. for $C_{29}H_{22}F_3N_3O_4$ (533.51): C, 65.29; H, 4.16; N, 7.88; found; C, 65.34; H, 4.23; N, 7.71.

*4.1.1.6. N-(4-Nitrophenyl)-2-(2-phenyl-N-(p-tolyl)acetamido)-2-(4-(trifluoromethyl)phenyl)-acetamide (**10**).* Off-white powder (72% yield), m.p = 233–235 °C; R_f = 0.54 (EtOAc : *n*-hexane, 1 : 2); IR (KBr, cm^{-1}): 3295 (N–H), 1635 (OCN); ^{1}H NMR (500 MHz, DMSO-d_6) δ_H: 10.94 (s, 1H, D_2O exchangeable, N–**H**), 8.19 (d, 2H, J = 9.0 Hz, Ar–**H**), 7.82 (d, 2H, J = 9.0 Hz, Ar–**H**), 7.52 (d, 2H, J = 8.5 Hz, Ar–**H**), 7.34 (d, 2H, J = 8.5 Hz, Ar–**H**), 7.22–7.13 (m, 4H, Ar–**H**), 7.02–7.01 (m, 5H, Ar–**H**), 6.26 (s, 1H, NC**H**CO), 3.37 (overlap with solvent peak, 2H, C**H**$_2$), 2.15 (s, 3H, C**H**$_3$); ^{13}C NMR (125 MHz, DMSO-d_6) δ_C: 171.3, 169.7(CON), 145.4, 142.9, 139.0, 138.0, 136.9, 135.9, 131.7, 131.1, 129.8, 129.7, 128.6, 126.9, 125.6, 119.5 (Ar–C), 125.5 (**C**F_3), 64.8 (N**C**HCO), 41.0 (**C**H_2), 21.1 (**C**H_3); anal. calc. for $C_{30}H_{24}F_3N_3O_4$ (547.53): C, 65.81; H, 4.42; N, 7.67; found C, 65.62; H, 4.51; N, 7.42.

*4.1.1.7. N-(2-((2-((4-Nitrophenyl)amino)-2-oxo-1-(4-(trifluoromethyl)phenyl)ethyl)(phenyl)amino)-2-oxoethyl) benzamide (**11**).* Off-white powder (60% yield), m.p = 260–262 °C; R_f = 0.48 (EtOAc : *n*-hexane, 1 : 2); IR (KBr, cm^{-1}): 3371 (N–H), 1702, 1675 (OCN); ^{1}H NMR (500 MHz, DMSO-d_6) δ_H: 10.99 (s, 1H, D_2O exchangeable, CON–**H**), 8.64 (t, 1H, J = 5.5 Hz, D_2O exchangeable, COCH$_2$N–**H**), 8.20 (d, 2H, J = 9.0 Hz, Ar–**H**), 7.84–7.79 (m, 4H, Ar–**H**), 7.53–7.47 (m, 4H, Ar–**H**), 7.43–7.36 (m, 5H, Ar–**H**), 7.22–7.19 (m, 3H, Hz, Ar–H), 6.27 (s, 1H, NC**H**CO), 3.87, 3.84 (dd, 1H, J = 16.5 Hz, J = 6.0 Hz 1H, C**H**$_a$H$_b$), 3.58, 3.55 (dd, 1H J = 17.5 Hz, J = 5.5 Hz, CH$_a$**H**$_b$); ^{13}C NMR (125 MHz, DMSO-d_6) δ_C: 169.5, 169.4, 166.8 (CON), 145.4, 142.9, 138.4, 134.3, 131.9, 131.7, 131.2, 129.6, 129.0, 128.8, 127.7, 119.5 (Ar–C), 125.6 (**C**F_3), 64.9 (N**C**HCO), 42.7 (N**C**H$_2$); anal. calc. for $C_{30}H_{23}F_3N_4O_5$ (576.53); C, 62.50; H, 4.02; N, 9.72; found C, 62.73; H, 3.93; N, 9.88.

*4.1.1.8. N-(2-((2-((4-Nitrophenyl)amino)-2-oxo-1-(4-(trifluoromethyl)phenyl)ethyl)(p-tolyl)amino)-2-oxoethyl)benzamide (**12**).* Off-white powder (55% yield), m.p = 258–260 °C; R_f = 0.46 (EtOAc : *n*-hexane, 1 : 2); IR (KBr, cm^{-1}): 3379 (N–H), 1676, 1641 (OCN); ^{1}HNMR (500 MHz, DMSO-d_6) δ_H: 10.98 (s, 1H, D_2O exchangeable, CON–**H**), 8.62 (t, 1H, J = 5.0 Hz, D_2O exchangeable, COCH$_2$N–**H**), 8.19 (d, 2H, J = 9.5 Hz, Ar–**H**), 7.83–7.79 (m, 4H, Ar–**H**), 7.55 (d, 3H, J = 8.5 Hz, Ar–**H**), 7.49 (t, 1H, J = 7.0 Hz, Ar–**H**), 7.42–7.36 (m, 5H, Ar–**H**), 7.06 (bs, 2H, Ar–**H**), 6.25 (s, 1H, NC**H**CO), 3.84, 3.81 (dd, 1H, J = 17.0 Hz, J = 6.0 Hz, C**H**$_a$H$_b$), 3.57, 3.53 (dd, 1H, J = 17.5 Hz, J = 5.0 Hz, CH$_a$**H**$_b$), 2.18 (s, 3H, C**H**$_3$); ^{13}C NMR (125 MHz, DMSO-d_6) δ_C: 169.6, 169.5, 166.8(CON), 145.4, 142.5, 138.5, 138.4, 135.7, 135.4, 132.0, 131.7, 130.9, 130.1, 128.8, 127.7, 119.5 (Ar–C), 125.6 (**C**F_3), 64.9 (N**C**HCO), 42.6 (CO**C**H_2), 21.1(**C**H_3); anal. calc. for $C_{31}H_{25}F_3N_4O_5$ (590.56); C, 63.05; H, 4.27; N, 9.49. Found; C, 63.21; H, 4.31; N, 9.30.

*4.1.1.9. N-(4-Nitrophenyl)-2-(N-phenyl-2-(phenylsulfonamido) acetamido)-2-(4-(trifluoromethyl)-phenyl)acetamide (**13**).* Off-white powder (75% yield), m.p = 223–225 °C; R_f = 0.45 (EtOAc : *n*-hexane, 1 : 2); IR (KBr, cm^{-1}): 3253 (N–H), 1666, 1620

(OCN); ^{1}H NMR (500 MHz, DMSO-d_6) δ_H: 10.94 (s, 1H, D_2O exchangeable, CON–**H**), 8.20 (d, 2H, J = 9.0 Hz, Ar–**H**), 7.94–7.89 (m, 1H, D_2O exchangeable, CH_2 N–**H**–SO_2), 7.81 (d, 2H, J = 9.0 Hz, Ar–**H**), 7.63 (d, 2H, J = 7.5 Hz, Ar–**H**), 7.57–7.47 (m, 6H, Ar–**H**), 7.26–7.16 (m, 6H, Ar–**H**), 6.14 (s, 1H, NC**H**CO), 3.38 (overlap with solvent peak, 2H, NC**H$_2$**); ^{13}C NMR (125 MHz, DMSO-d_6) δ_C: 169.2, 168.0 (CON), 145.3, 143.0, 140.7, 138.2, 137.8, 133.0, 131.6, 131.1, 129.6, 129.2, 127.1, 126.9, 119.5 (Ar–C), 125.6 (**C**F$_3$), 64.7 (N**C**HCO), 45.1 (NCH$_2$); anal. calc. for $C_{29}H_{23}F_3N_4O_6S$ (612.58): C, 56.86; H, 3.78; N, 9.15; found; C, 56.93; H, 3.92; N, 9.18.

*4.1.1.10. N-(4-Nitrophenyl)-2-(2-(phenylsulfonamido)-N-(p-tolyl)acetamido)-2-(4-(trifluoromethyl)-phenyl)acetamide (**14**).* Pale yellow powder (80% yield), m.p = 245–247 °C; R_f = 0.5 (EtOAc : *n*-hexane, 1 : 2); IR (KBr, cm^{-1}): 3254 (N–H), 1666, 1617 (OCN); ^{1}H NMR (500 MHz, DMSO-d_6) δ_H: 10.91 (s, 1H, D_2O exchangeable, CON–**H**), 8.20 (d, 2H, J = 9.0 Hz, Ar–**H**), 7.92 (bs, 1H, D_2O exchangeable, CH_2 N–**H**–SO_2), 7.80 (d, 2H, J = 9.0 Hz, Ar–**H**), 7.64 (d, 2H, J = 7.0 Hz, Ar–**H**), 7.57–7.48 (m, 8H, Ar–**H**) 7.25 (d, 2H, J = 8.5 Hz, Ar–**H**), 6.98 (bs, 1H, Ar–**H**) 6.12 (s, 1H, NC**H**CO), 3.36 (overlap with solvent peak, 2H, NC**H$_2$**), 2.14 (s, 3H, C**H$_3$**); ^{13}C NMR (125 MHz, DMSO-d_6) δ_C: 169.2, 168.2 (CON), 145.3, 143.0, 140.8, 138.5, 138.3, 135.2, 132.9, 131.6, 130.8, 130.0, 129.6, 129.3, 129.1, 126.9, 123.3, 119.5 (Ar–C), 125.6 (**C**F$_3$), 64.6 (N**C**HCO), 45.1 (N**C**H$_2$), 21.1 (**C**H$_3$); anal. calc. for $C_{30}H_{25}F_3N_4O_6S$: (626.61); C, 57.50; H, 4.02; N, 8.94; found; C, 57.71; H, 4.33; N, 8.84.

*4.1.1.11. N-Benzyl-N-(2-((4-nitrophenyl)amino)-2-oxo-1-(4-(trifluoromethyl)phenyl)-ethyl)-2-phenyl-acetamide (**15**).* Off-white powder (70% yield), m.p = 170–172 °C; R_f = 0.57 (EtOAc : *n*-hexane, 1 : 2); IR (KBr, cm^{-1}): 3288 (N–H), 1708, 1630 (OCN); ^{1}HNMR (500 MHz, DMSO-d_6) δ_H: 10.93 (s, 1H, D_2O exchangeable, CON–**H**), 8.17 (d, 2H, J = 8.5 Hz, Ar–**H**), 7.75 (d, 2H, J = 9.0 Hz, Ar–**H**), 7.54–7.44 (m, 4H, Ar–**H**), 7.26–7.07 (m, 8H, Ar–**H**), 6.98–6.93 (m, 2H, Ar–**H**), 6.24 (s, 1H, NC**H**CO), 4.84 (d, 1H, J = 18.5 Hz, NC**H$_a$**H$_b$Ph), 4.58 (d, 1H, J = 18.5 Hz, NCH$_a$**H$_b$**Ph), 3.75 (q, 2H, J = 15.5 Hz, COC**H$_2$**Ph); ^{13}C NMR (125 MHz, DMSO-d_6) δ_C: 172.9, 169.4 (CON), 145.3, 142.9, 138.3, 135.7, 131.1, 129.9, 129.8, 128.7, 128.6, 127.2, 127.0, 126.4, 125.8, 125.7, 119.6 (Ar–C), 125.5 (**C**F$_3$), 62.7 (N**C**HCO), 49.4 (N**C**H$_2$), 40.4 (under solvent peak COCH$_2$); anal. calc. for $C_{30}H_{24}F_3N_3O_4$ (547.53): C, 65.81; H, 4.42; N, 7.67; found; C, 66.07; H, 4.52; N, 7.54.

*4.1.1.12. N-(2-(Benzyl(2-((4-nitrophenyl)amino)-2-oxo-1-(4-(trifluoromethyl)phenyl)ethyl)amino)-2-oxoethyl)benzamide (**16**).* Off-white powder (60% yield), m.p = 258–260 °C; R_f = 0.46 (EtOAc : *n*-hexane, 1 : 2); IR (KBr, cm^{-1}): 3414 (N–H), 1707, 1643 (OCN); ^{1}HNMR (500 MHz, DMSO-d_6) δ_H: 10.92 (s, 1H, D_2O exchangeable, CON–**H**), 8.78 (t, 1H, J = 6.0, D_2O exchangeable, CH_2N–**H**), 8.17 (d, 2H, J = 9.0 Hz, Ar–**H**), 7.84 (d, 2H, J = 7.5 Hz, Ar–**H**), 7.75 (d, 2H, J = 9.0 Hz, Ar–**H**), 7.55–7.41 (m, 5H, Ar–**H**), 7.24–7.21 (m, 1H, Ar–**H**), 7.14–7.05 (m, 6H, Ar–**H**), 6.21 (s, 1H, NC**H**CO), 4.88 (d, 1H, J = 17.5 Hz, NC**H$_a$**H$_b$), 4.59 (d, 1H, J = 18.5 Hz, NCH$_a$**H$_b$**), 4.13–4.18 (2d, 1H, J = 7.5 Hz, J = 14.0 Hz, COC**H$_2$**), 4.01–3.96 (m, 1H, COC**H$_2$**); ^{13}C NMR (125 MHz, DMSO-d_6) δ_C: 171.1, 169.3, 167.3 (CON), 145.2, 142.9, 137.9, 134.3, 132.0, 131.1, 128.9, 128.7, 128.6, 127.9, 127.7, 126.5, 125.7, 119.6 (Ar–C), 125.5 (**C**F$_3$), 62.9 (N**C**HCO), 48.7 (NCH$_2$), 42.3 (CO**C**H$_2$); anal. calc. for $C_{31}H_{25}F_3N_4O_5$ (590.56); C, 63.05; H, 4.27; N, 9.49; found; C, 63.22; H, 4.44; N, 9.31.

*4.1.1.13. N-Benzyl-N-(2-((4-nitrophenyl)amino)-2-oxo-1-(4-(trifluoromethyl)phenyl)ethyl)-2-(phenylsulfonamido)acetamide (**17**).* White powder (61% yield), m.p = 197–199 °C; R_f = 0.54 (EtOAc : *n*-hexane, 1 : 2); IR (KBr, cm^{-1}): 3296 (N–H), 1706, 1644 (OCN); ^{1}H NMR (500 MHz, DMSO-d_6) δ_H: 10.89 (s, 1H, D_2O exchangeable, CON–**H**), 8.18 (d, 2H, J = 9.0 Hz, Ar–**H**), 7.98 (bs, 1H, D_2O exchangeable CH_2 N–**H**–SO_2), 7.75 (d, 2H, J = 9.0 Hz, Ar–**H**), 7.63 (d, 2H, J = 7.5 Hz, Ar–**H**), 7.56 (d, 3H, J = 8.0 Hz, Ar–**H**), 7.49 (t, 2H, J = 7.5 Hz, Ar–**H**), 7.39 (d, 2H, J = 7.5 Hz, Ar–**H**), 7.10–7.09 (m, 2H, Ar–**H**), 6.94–6.74 (m, 3H, Ar–**H**), 6.16 (s, 1H, NC**H**CO), 4.69 (d, 1H, J = 18.0 Hz, C**H$_a$**H$_b$ NPh), 4.48 (d, 1H, J = 18.0 Hz, CH$_a$**H$_b$** NPh), 3.80 (d, 1H, J = 17.5 Hz, C**H$_a$**H$_b$ NHSO$_2$Ph), 3.68 (d, 1H, J = 17.5 Hz CH$_a$**H$_b$** NHSO$_2$Ph); ^{13}C NMR (125 MHz, DMSO-d_6) δ_C: 169.9, 169.0 (CON), 145.2, 143.0, 140.8, 139.1, 137.7, 132.9, 131.1, 129.5, 128.7, 127.3, 127.2, 127.1, 126.3, 125.8, 119.7 (Ar–C), 125.5 (**C**F$_3$), 62.8 (N**C**HCO), 48.5 (N**C**H$_2$Ph), 45.1 (**C**H$_2$NH SO$_2$Ph); anal. calc. for $C_{30}H_{25}F_3N_4O_6S$ (626.61): C, 57.50; H, 4.02; N, 8.94; found; C, 57.77; H, 4.21; N, 8.81.

*4.1.1.14. N-(2-((4-Nitrophenyl)amino)-2-oxo-1-(4-(trifluoromethyl)phenyl)ethyl)-N-phenylquinoline-2-carboxamide (**18**).* White powder (66% yield), m.p = 231–233 °C; R_f = 0.628 (EtOAc : *n*-hexane, 1 : 2); IR (KBr, cm^{-1}): 3265 (N–H), 1673, 1631 (OCN); ^{1}H NMR (500 MHz, DMSO-d_6) δ_H: 11.15 (bs, 1H, D_2O exchangeable N–**H**), 8.23 (d, 3H, J = 9.0 Hz, Ar–**H**), 7.89 (d, 2H, J = 9.5 Hz, Ar–**H**), 7.84 (d, 1H, J = 8.5 Hz, Ar–**H**), 7.74 (d, 1H, J = 8.5 Hz, Ar–**H**), 7.66 (t, 1H, J = 7.0 Hz, Ar–**H**), 7.57–7.47 (m, 6H, Ar–**H**), 7.13 (bs, 2H, Ar–**H**), 6.88–6.83 (m, 3H, Ar–**H**), 6.53 (s, 1H, NC**H**CO); ^{13}C NMR (125 MHz, DMSO-d_6) δ_C: 169.3, 168.9 (CON), 145.4, 143.0, 140.5, 139.2, 138.5, 137.0, 136.9, 131.8, 131.6, 130.6, 129.3, 129.2, 128.4, 128.3, 128.0, 127.9, 127.5, 120.6, 119.6, 119.5 (Ar–C), 125.6 (**C**F$_3$), 65.1 (N**C**HCO); anal. calc. for $C_{31}H_{21}F_3N_4O_4$ (570.53): C, 65.26; H, 3.71; N, 9.82. Found; C, 65.45; H, 3.83; N, 9.59.

*4.1.1.15. N-(2-((4-Nitrophenyl)amino)-2-oxo-1-(4-(trifluoromethyl)phenyl)ethyl)-N-(p-tolyl)-quinoline-2-carboxamide (**19**).* White powder (63% yield), m.p = 213–215 °C; R_f = 0.628 (EtOAc : *n*-hexane, 1 : 2); IR (KBr, cm^{-1}): 3268 (N–H), 1672, 1635 (OCN); ^{1}H NMR (500 MHz, DMSO-d_6) δ_H: 11.13 (bs, 1H, D_2O exchangeable, N–**H**), 8.22 (d, 3H, J = 9.0 Hz, Ar–**H**), 7.89 (d, 2H, J = 8.5 Hz, Ar–**H**), 7.84 (d, 1H, J = 7.5 Hz, Ar–**H**), 7.79 (d, 1H, J = 8.5 Hz, Ar–**H**), 7.67 (t, 1H, J = 7.5 Hz, Ar–**H**), 7.59–7.47 (m, 6H, Ar–**H**), 7.01 (bs, 2H, Ar–**H**), 6.69 (d, 2H, J = 7.0 Hz, Ar–**H**), 6.51 (s, 1H, NC**H**CO), 1.90 (s, 3H, C**H$_3$**). ^{13}C NMR (125 MHz, DMSO-d_6) δ_C: 169.3, 169.1 (CON), 154.8, 146.6, 145.4, 143.0, 137.2, 137.0, 136.5, 131.8, 131.4, 130.7, 129.3, 128.9, 128.4, 128.0, 127.5, 125.6, 120.6, 119.6 (Ar–C), 125.5 (**C**F$_3$), 65.7 (N**C**HCO), 20.9 (**C**H$_3$); anal. calc. for $C_{32}H_{23}F_3N_4O_4$ (584.56): C, 65.75; H, 3.97; N, 9.58. Found; C, 65.88; H, 4.19; N, 9.30.

*4.1.1.16. {R,S}N-Benzyl-N-(2-((4-nitrophenyl)amino)-2-oxo-1-(4-(trifluoromethyl)phenyl)ethyl)-quinoline-2-carboxamide (**20**).* White powder (80% yield), m.p = 231–233 °C; R_f = 0.628 (EtOAc : *n*-hexane, 1 : 2); IR (KBr, cm^{-1}): 3278 (N–H), 1618 (OCN); ^{1}H NMR (500 MHz, DMSO-d_6) δ_H: 11.05, 10.60(2s, 1H, D_2O exchangeable N–**H**), 8.57, 8.39 (2d, 1H, J = 8.5 Hz, J = 8.5 Hz Ar–**H**), 8.21 (t, 2H, J = 8.5 Hz, Ar–**H**), 8.061 (d, 1H, J =

8.0 Hz, Ar–**H**), 7.96–7.89 (m, 1H, Ar–**H**), 7.84 (d, 1H, J = 8.0 Hz, Ar–**H**), 7.75–7.62 (m, 4H, Ar–**H**), 7.56–7.48 (m, 4H, Ar–**H**), 7.24–7.21, 7.14–7.09 (2m, 1H, Ar–**H**), 6.99 (s, 1H, Ar–**H**), 6.91 (s, 3H, Ar–**H**), 6.32, 6.25(2s, 1H, NC**H**CO) 5.21, 4.97(2d, 1H, J = 16 Hz, J = 17 Hz C$\mathbf{H}_a$H$_b$ – N-Ph), 4.63, 4.44 (2d, 1H, J = 17 Hz, J = 15 Hz, CH$_a$**H**$_b$ N-Ph); ^{13}C NMR (125 MHz, DMSO-d_6) δ_C: 170.3, 169.6, 169.5, 169.0 (CON), 153.9, 153.6, 146.2, 146.1, 145.3, 145.1, 143.0, 139.3, 138.8, 138.7, 138.5, 138.2, 138.0, 131.3, 131.1, 131.0, 130.9, 129.5, 129.4, 128.8, 128.7, 128.6, 128.5, 128.4, 128.0, 127.9,127.3, 126.5, 126.3, (Ar–C), 121.7, 120.9, 119.7, 119.6 (Ar–C), 125.7, 125.6, 125.5 (**C**F$_3$) , 65.5, 63.1 (N**C**HCO), 51.2, 48.8 (**C**H$_2$); anal. calc. for $C_{32}H_{23}F_3N_4O_4$ (584.56): C, 65.75; H, 3.97; N, 9.58, found; C, 65.82; H, 9.84; N, 9.39.

4.1.2. The general method for the synthesis of ugi adducts: (23–25). A mixture of benzaldehyde **21** (0.743 mmol) and aniline derivatives **2a–b** (0.743 mmol), or benzylamine **2c** (0.743 mmol) in ethanol (2 ml) was stirred under reflux for 1 h then, 4-(trifluoromethyl) cinnamic acid **22** (0.67 mmol), isonitrile **3** (0.67 mmol) and TFE (2 ml) were added to the reaction mixture. Stirring continued under reflux for 5 has monitored by TLC. The crude obtained was filtered off, washed with ethanol, dried, and crystallized from ethanol.

*4.1.2.1. (E)-N-(2-((4-Nitrophenyl)amino)-2-oxo-1-phenylethyl)-N-phenyl-3-(4-(trifluoromethyl)-phenyl)acrylamide (**23**).* Off-white powder (65% yield), m.p = 247–249 °C; R_f = 0.46 (EtOAc : *n*-hexane, 1 : 2); IR (KBr, cm^{-1}): 3445 (N–H), 1654 (OCN); ^{1}HNMR (500 MHz, DMSO-d_6) δ_H: 10.98 (s, 1H, D$_2$O exchangeable, CON**H**), 8.20 (d, 2H, J = 9.0 Hz, Ar–**H**), 7.86 (d, 2H, J = 9.5 Hz, Ar–**H**), 7.65 (d, 2H, J = 8.5 Hz, Ar–**H**), 7.60 (d, 1H, J = 15.0, CH=CH) 7.50 (d, 2H, J = 8.0 Hz, Ar–**H**), 7.18–7.12 (m, 10H, Ar–**H**), 6.30 (s, 1H, NC**H**CO), 6.23 (d, 1H, J = 15.5, CH=CH); ^{13}C NMR (125 MHz, DMSO-d_6) δ_C: 170.3, 165.4(CON), 145.7, 142.8, 140.2, 139.0, 138.9, 133.8, 131.6, 130.8, 129.2, 128.9, 128.8, 128.7, 126.4, 126.3, 122.2, 119.4 (Ar–C + CH=CH), 125.6 (**C**F$_3$), 65.6 (N**C**HCO); anal. calc. for $C_{30}H_{22}F_3N_3O_4$ (545.52): C, 66.05; H, 4.07; N, 7.70; found; C, 65.91; H, 4.23; N, 7.61.

*4.1.2.2. (E)-N-(2-((4-Nitrophenyl)amino)-2-oxo-1-phenylethyl)-N-(p-tolyl)-3-(4-(trifluoromethyl)-phenyl)acrylamide (**24**).* Off-white powder (84% yield), m.p = 227–229 °C; R_f = 0.36 (EtOAc : *n*-hexane, 1 : 2); IR (KBr, cm^{-1}): 3442 (N–H), 1660 (OCN); ^{1}HNMR (500 MHz, DMSO-d_6) δ_H: 10.96 (s, 1H, D$_2$O exchangeable, CON–**H**), 8.20 (d, 2H, J = 9.0 Hz, Ar–**H**), 7.86 (d, 2H, J = 9.0 Hz, Ar–**H**), 7.66 (d, 2H, J = 8.5 Hz, Ar–**H**), 7.60 (d, 1H, J = 16.0 Hz CH=CH) 7.51 (d, 2H, J = 8.0 Hz, Ar–**H**), 7.14–7.12 (m, 7H, Ar–**H**), 6.99 (bs, 2H, Ar–**H**), 6.28 (s, 1H, NC**H**CO) 6.27 (d, 1H, J = 16.0 Hz, CH=CH), 2.17 (s, 3H, C**H**$_3$); ^{13}C NMR (125 MHz, DMSO-d_6) δ_C: 170.3, 165.0 (CON), 145.7, 142.8, 140.2, 139.0, 137.8, 136.3, 133.9, 131.2, 130.9, 129.7, 128.9, 128.8, 126.4, 122.3, 119.3 (Ar–C + CH=CH), 125.6 (**C**F$_3$), 65.6 (N**C**HCO), 21.1 (**C**H$_3$); anal. calc. for $C_{31}H_{24}F_3N_3O_4$ (559.55): C, 66.54; H, 4.32; N, 7.51; found; C, 66.78; H, 4.29; N, 7.45.

*4.1.2.3. (E)-N-Benzyl-N-(2-((4-nitrophenyl)amino)-2-oxo-1-phenylethyl)-3-(4-(trifluoromethyl)-phenyl)acrylamide (**25**).* Off-white powder (65% yield), m.p = 245–247 °C; R_f = 0.43 (EtOAc : *n*-hexane, 1 : 2); IR (KBr, cm^{-1}): 3445 (N–H), 1652 (OCN); ^{1}HNMR (500 MHz, DMSO-d_6) δ_H: 10.93 (s, 1H, D$_2$O exchangeable, CON–**H**), 8.19 (d, 2H, J = 9.0 Hz, Ar–**H**), 7.81 (d, 2H, J = 9.0 Hz, Ar–**H**), 7.75–7.66 (m, 4H, Ar–**H**), 7.64 (d, 1H, J = 15.0 Hz, CH=CH), 7.27–7.23 (m, 5H, Ar–**H**), 7.11–7.09 (m, 3H, Ar–**H**), 7.06–7.03 (m, 1H, Ar–**H**), 6.96 (d, 2H, J = 7.5 Hz, Ar–**H** + CH=CH), 6.28 (s, 1H, NC**H**CO), 5.04 (d, 1H, J = 17.5 Hz, NC$\mathbf{H}_a$H$_b$Ph), 4.6 (d, 1H, J = 17.5 Hz, NCH$_a$**H**$_b$ Ph); ^{13}C NMR (125 MHz, DMSO-d_6) δ_C: 170.2, 167.4 (CON), 145.5, 142.8, 141.2, 139.4, 134.4, 130.4, 129.1, 128.5, 127.1, 126.5, 126.1, 122.2, 119.4 (Ar–C + CH=CH), 125.6 (**C**F$_3$), 63.6 (N**C**HCO), 48.7 (N**C**H$_2$); anal. calc. for $C_{31}H_{24}F_3N_3O_4$ (559.55); C, 66.54; H, 4.32; N, 7.51. Found; C, 66.37; H, 4.12; N, 7.68.

4.2. Biological evaluation

The biological assays were carried out according to the previously reported procedures and have been provided in the ESI;† anti-proliferative activity assay,[70] EGFR inhibition assays,[81,82] mRNA expression assay,[83] and caspase-3/9 activation assay.[84]

4.3. Molecular docking studies

The X-ray crystallographic structures of Wild-type EGFR (PDB: 1M17)[80] and mutant EGFR enzyme (PDB: 6LUB),[80] with resolutions of 2.60 Å and 2.31 Å, respectively, were obtained from the RCSB Protein Data Bank (**http://www.pdb.org**). Molecular modeling was performed using the Molecular Operating Environment (MOE 2022.09; Chemical Computing Group, Canada) software. Hydrogen atoms were added, and the protonation states of amino acid residues were assigned using the Protonate 3D algorithm.[85] The compounds were modeled guided with the X-ray experiment of the compounds, followed by energy minimization using the MMFF94× force field. Docking studies of the synthesized compound were conducted using the MOE Dock tool, and the final ligand–enzyme complexes were selected based on interaction energy and geometric matching quality.

Data availability

Data for this article, including [description of IR, NMR, experimental, elemental analysis, and methodology and docking software] are available in the attached ESI† pdf file.

Conflicts of interest

The authors declare no conflict of interest.

Funding

This work was supported by the Deanship of Scientific Research, Vice Presidency for Graduate Studies and Scientific Research, King Faisal University, Saudi Arabia, under the annual funding track [KFU250646].

Acknowledgements

MSA acknowledges "the Deanship of Scientific Research, Vice Presidency for Graduate Studies and Scientific Research, King Faisal University, Saudi Arabia, for financial support under the annual funding track [KFU250646]".

References

1 G. B. of D. C. Collaboration, *JAMA Oncol.*, 2019, **5**, 1749–1768.
2 H. Sung, J. Ferlay, R. L. Siegel, M. Laversanne, I. Soerjomataram, A. Jemal and F. Bray, *Ca-Cancer J. Clin.*, 2021, **71**, 209–249.
3 F. Bray, M. Laversanne, E. Weiderpass and I. Soerjomataram, *Cancer*, 2021, **127**, 3029–3030.
4 F. Bray, M. Laversanne, H. Sung, J. Ferlay, R. L. Siegel, I. Soerjomataram and A. Jemal, *Ca-Cancer J. Clin.*, 2024, **74**, 229–263.
5 D. Hanahan and R. A. Weinberg, *Cell*, 2011, **144**, 646–674.
6 A. F. Chambers, A. C. Groom and I. C. MacDonald, *Nat. Rev. Cancer*, 2002, **2**, 563–572.
7 A. W. Lambert, D. R. Pattabiraman and R. A. Weinberg, *Cell*, 2017, **168**, 670–691.
8 N. V. Krakhmal, M. V. Zavyalova, E. V. Denisov, S. V. Vtorushin and V. M. Perelmuter, *Cancer Invasion: Patterns and Mechanisms*, 2015, vol. 7.
9 A. G. Clark and D. M. Vignjevic, *Curr. Opin. Cell Biol.*, 2015, **36**, 13–22.
10 B. Rude Voldborg, L. Damstrup, M. Spang-Thomsen and H. Skovgaard Poulsen, *Ann. Oncol.*, 1997, **8**, 1197–1206.
11 J. Chen, F. Zeng, S. J. Forrester, S. Eguchi, M.-Z. Zhang and R. C. Harris, *Physiol. Rev.*, 2016, **96**, 1025–1069.
12 Md. Habban Akhter, N. Sateesh Madhav and J. Ahmad, *Artif. Cells, Nanomed., Biotechnol.*, 2018, **46**, 1188–1198.
13 S. I. Faggal, Y. El-Dash, A. Sonousi, A. M. Abdou and R. A. Hassan, *RSC Med. Chem.*, 2024, **15**(12), 4111–4125.
14 S. B. Kondapaka, R. Fridman and K. B. Reddy, *Int. J. Cancer*, 1997, **70**, 722–726.
15 R. S. Herbst, *Int. J. Radiat. Oncol., Biol., Phys.*, 2004, **59**, S21–S26.
16 M. A. Abdelgawad, R. B. Bakr, O. A. Alkhoja and W. R. Mohamed, *Bioorg. Chem.*, 2016, **66**, 88–96.
17 T. Le and D. E. Gerber, *Cancers*, 2019, **11**(3), 366.
18 J. Graham, M. Muhsin and P. Kirkpatrick, *Nat. Rev. Drug Discovery*, 2004, **3**(1), 11–12.
19 J. Dowell, J. D. Minna and P. Kirkpatrick, *Nat. Rev. Drug Discovery*, 2005, **4**, 13–14.
20 H. A. Yu, M. E. Arcila, N. Rekhtman, C. S. Sima, M. F. Zakowski, W. Pao, M. G. Kris, V. A. Miller, M. Ladanyi and G. J. Riely, *Clin. Cancer Res.*, 2013, **19**, 2240–2247.
21 D. Li, T. Shimamura, H. Ji, L. Chen, H. J. Haringsma, K. McNamara, M.-C. Liang, S. A. Perera, S. Zaghlul, C. L. Borgman, S. Kubo, M. Takahashi, Y. Sun, L. R. Chirieac, R. F. Padera, N. I. Lindeman, P. A. Jänne, R. K. Thomas, M. L. Meyerson, M. J. Eck, J. A. Engelman, G. I. Shapiro and K.-K. Wong, *Cancer Cell*, 2007, **12**, 81–93.
22 A. Y. Helena and G. J. Riely, *J. Natl. Compr. Cancer Network*, 2013, **11**, 161–169.
23 S. C. M. Lau, U. Batra, T. S. K. Mok and H. H. Loong, *Drugs*, 2019, **79**, 823–831.
24 Y. Kim, J. Ko, Z. Cui, A. Abolhoda, J. S. Ahn, S.-H. Ou, M.-J. Ahn and K. Park, *Mol. Cancer Ther.*, 2012, **11**, 784–791.
25 H.-N. Song, K. S. Jung, K. H. Yoo, J. Cho, J. Y. Lee, S. H. Lim, H. S. Kim, J.-M. Sun, S.-H. Lee, J. S. Ahn, K. Park, Y.-L. Choi, W. Park and M.-J. Ahn, *J. Thorac. Oncol.*, 2016, **11**, e45–e47.
26 D. A. E. Cross, S. E. Ashton, S. Ghiorghiu, C. Eberlein, C. A. Nebhan, P. J. Spitzler, J. P. Orme, M. R. V Finlay, R. A. Ward, M. J. Mellor, G. Hughes, A. Rahi, V. N. Jacobs, M. R. Brewer, E. Ichihara, J. Sun, H. Jin, P. Ballard, K. Al-Kadhimi, R. Rowlinson, T. Klinowska, G. H. P. Richmond, M. Cantarini, D.-W. Kim, M. R. Ranson and W. Pao, *Cancer Discovery*, 2014, **4**, 1046–1061.
27 T. Hirano, H. Yasuda, J. Hamamoto, S. Nukaga, K. Masuzawa, I. Kawada, K. Naoki, T. Niimi, S. Mimasu, H. Sakagami, K. Soejima and T. Betsuyaku, *Mol. Cancer Ther.*, 2018, **17**, 740–750.
28 Q. Wu, H. Jiang, S. Wang, D. Dai, F. Chen, D. Meng, P. Geng, H. Tong, Y. Zhou, D. Pan, Q. Zhou and C. Wang, *Thorac. Cancer*, 2020, **11**, 2775–2781.
29 S. Khozin, C. Weinstock, G. M. Blumenthal, J. Cheng, K. He, L. Zhuang, H. Zhao, R. Charlab, I. Fan, P. Keegan and R. Pazdur, *Clin. Cancer Res.*, 2017, **23**, 2131–2135.
30 C. Mehlman, J. Cadranel, G. Rousseau-Bussac, R. Lacave, A. Pujals, N. Girard, C. Callens, V. Gounant, N. Théou-Anton, S. Friard, J. Trédaniel, H. Blons, C. Dujon, B. Duchemann, P. O. Schischmanoff, T. Chinet and E. Giroux Leprieur, *Lung Cancer*, 2019, **137**, 149–156.
31 K. S. Thress, C. P. Paweletz, E. Felip, B. C. Cho, D. Stetson, B. Dougherty, Z. Lai, A. Markovets, A. Vivancos, Y. Kuang, D. Ercan, S. E. Matthews, M. Cantarini, J. C. Barrett, P. A. Jänne and G. R. Oxnard, *Nat. Med.*, 2015, **21**, 560–562.
32 T. Grabe, J. Lategahn and D. Rauh, *ACS Med. Chem. Lett.*, 2018, **9**, 779–782.
33 M. A. Mansour, A. M. AboulMagd, S. H. Abbas, H. M. Abdel-Rahman and M. Abdel-Aziz, *RSC Adv.*, 2023, **13**(27), 18825–18853.
34 Y. Jia, C. H. Yun, E. Park, D. Ercan, M. Manuia, J. Juarez, C. Xu, K. Rhee, T. Chen, H. Zhang, S. Palakurthi, J. Jang, G. Lelais, M. DiDonato, B. Bursulaya, P. Y. Michellys, R. Epple, T. H. Marsilje, M. McNeill, W. Lu, J. Harris, S. Bender, K. K. Wong, P. A. Jänne and M. J. Eck, *Nature*, 2016, **534**, 129–132.
35 H. Patel, R. Pawara, A. Ansari and S. Surana, *Eur. J. Med. Chem.*, 2017, **142**, 32–47.
36 S. Lee, J. Kim, K. B. Duggirala, A. Go, I. Shin, B. C. Cho, G. Choi, C. H. Chae and K. Lee, *Bull. Korean Chem. Soc.*, 2018, **39**, 895–898.
37 A. Esquela-Kerscher and F. J. Slack, *Nat. Rev. Cancer*, 2006, **6**, 259–269.
38 D. M. Pereira, P. M. Rodrigues, P. M. Borralho and C. M. P. Rodrigues, *Drug Discovery Today*, 2013, **18**, 282–289.
39 D. Baltimore, M. P. Boldin, R. M. O'Connell, D. S. Rao and K. D. Taganov, *Nat. Immunol.*, 2008, **9**, 839–845.
40 R. H. A. Plasterk, *Cell*, 2006, **124**, 877–881.
41 F. Han, J. He, F. Li, J. Yang, J. Wei, W. C. Cho and X. Liu, *BioMed Res. Int.*, 2015, **2015**(1), 672759.
42 J. Li, J. H. Huang, J. Y. Wang, Z. G. Xu, Z. Z. Chen and J. Lei, *RSC Adv.*, 2022, **12**, 33175–33179.

43 F. Tahoori, R. Sheikhnejad, S. Balalaie and M. Sadjadi, *Amino Acids*, 2013, **45**, 975–981.
44 N. Seixas, B. B. Ravanello, I. Morgan, G. N. Kaluderovic and L. A. Wessjohann, *Pharmaceutics*, 2019, **11**(2), 59.
45 J. Wiemann, L. Fischer, J. Kessler, D. Ströhl and R. Csuk, *Bioorg. Chem.*, 2018, **81**, 567–576.
46 J. N. Gohel, K. S. Lunagariya, K. M. Kapadiya and R. C. Khunt, *ChemistrySelect*, 2018, **3**, 11657–11662.
47 P. Brandão, A. Puerta, J. M. Padrón, M. L. Kuznetsov, A. J. Burke and M. Pineiro, *Asian J. Org. Chem.*, 2021, **10**, 3434–3455.
48 S. De Castro, M. J. Camarasa, J. Balzarini and S. Velázquez, *Eur. J. Med. Chem.*, 2014, **83**, 174–189.
49 M. S. Ayoup, M. A. Fouad, H. Abdel-Hamid, E. S. Ramadan, M. M. Abu-Serie, A. Noby and M. Teleb, *Eur. J. Med. Chem.*, 2020, **186**, 111875.
50 M. S. Ayoup, Y. Wahby, H. Abdel-Hamid, M. M. Abu-Serie, S. Ramadan, A. Barakat, M. Teleb and M. M. F. Ismail, *RSC Adv.*, 2023, **13**, 27722–27737.
51 F. R. Leroux, B. Manteau, J.-P. Vors and S. Pazenok, *Beilstein J. Org. Chem.*, 2008, **4**, 13.
52 O. S. Artamonov, E. Y. Slobodyanyuk, D. M. Volochnyuk, I. V. Komarov, A. A. Tolmachev and P. K. Mykhailiuk, *Eur. J. Org. Chem.*, 2014, **2014**, 3592–3598.
53 F. M. Sroor, K. F. Mahrous, H. A. M. A. El-Kader, A. M. Othman and N. S. Ibrahim, *Sci. Rep.*, 2023, **13**, 17560.
54 J. Lei, J.-P. Meng, D.-Y. Tang, B. Frett, Z.-Z. Chen and Z.-G. Xu, *Mol. Diversity*, 2018, **22**, 503–516.
55 Z. Xu, F. De Moliner, A. P. Cappelli and C. Hulme, *Angew Chem. Int. Ed. Engl.*, 2012, **51**, 8037.
56 R. J. Glyn and G. Pattison, *J. Med. Chem.*, 2021, **64**, 10246–10259.
57 H. L. Yale, *J. Med. Pharm. Chem.*, 1959, **1**, 121–133.
58 E. J. Cho, T. D. Senecal, T. Kinzel, Y. Zhang, D. A. Watson and S. L. Buchwald, *Science*, 2010, **328**, 1679–1681.
59 N. A. Meanwell, *J. Med. Chem.*, 2011, **54**, 2529–2591.
60 Q. Wang, L. He, K. K. Li and G. C. Tsui, *Org. Lett.*, 2017, **19**, 658–661.
61 S. Schiesser, H. Chepliaka, J. Kollback, T. Quennesson, W. Czechtizky and R. J. Cox, *J. Med. Chem.*, 2020, **63**, 13076–13089.
62 M. Krátký, K. Svrčková, Q. A. Vu, Š. Štěpánková and J. Vinšová, *Molecules*, 2021, **26**, 989.
63 Y. Saito, A. Mizokami, K. Izumi, R. Naito, M. Goto and K. Nakagawa-Goto, *Molecules*, 2021, **26**, 2812.
64 A. Abula, Z. Xu, Z. Zhu, C. Peng, Z. Chen, W. Zhu and H. A. Aisa, *J. Chem. Inf. Model.*, 2020, **60**, 6242–6250.
65 H. S. Rugo, F. Lerebours, E. Ciruelos, P. Drullinsky, M. Ruiz-Borrego, P. Neven, Y. H. Park, A. Prat, T. Bachelot, D. Juric, N. Turner, N. Sophos, J. P. Zarate, C. Arce, Y.-M. Shen, S. Turner, H. Kanakamedala, W.-C. Hsu and S. Chia, *Lancet Oncol.*, 2021, **22**, 489–498.
66 C. Möller, W. Bone, A. Cleve, U. Klar, A. Rotgeri, A. Rottmann, M.-H. Schultze-Mosgau, A. Wagenfeld and W. Schwede, *ChemMedChem*, 2018, **13**, 2271–2280.
67 S. R. Nasrin, T. Ishihara, A. M. R. Kabir, A. Konagaya, K. Sada and A. Kakugo, *Polym. J.*, 2020, **52**, 969–976.
68 C. Helsen, T. Van den Broeck, A. Voet, S. Prekovic, H. Van Poppel, S. Joniau and F. Claessens, *Endocr.-Relat. Cancer*, 2014, **21**, T105–T118.
69 S. M. Wilhelm, C. Carter, L. Tang, D. Wilkie, A. McNabola, H. Rong, C. Chen, X. Zhang, P. Vincent and M. McHugh, *Cancer Res.*, 2004, **64**, 7099–7109.
70 T. Mosmann, *J. Immunol. Methods*, 1983, **65**, 55–63.
71 X. Ma, J. Huang, Y. Tian, Y. Chen, Y. Yang, X. Zhang, F. Zhang and L. Xue, *Oncogene*, 2017, **36**, 3159–3167.
72 G. Y. Liou, *Int. J. Biochem. Cell Biol.*, 2019, **106**, 1–7.
73 K. S. Nam, S. Oh, K. Lee, S. Yoo and I. Shin, *Cell Signal*, 2015, **27**, 1882–1894.
74 R. Bhattacharya, F. Fan, R. Wang, X. Ye, L. Xia, D. Boulbes and L. M. Ellis, *Br. J. Cancer*, 2017, **117**, 848–855.
75 Y. Zhao, J. Ma, Y. Fan, Z. Wang, R. Tian, W. Ji, F. Zhang and R. Niu, *Mol. Oncol.*, 2018, **12**, 305–321.
76 L. Chen, Q. Zhu, L. Lu and Y. Liu, *Bioengineered*, 2020, **11**, 91–102.
77 S. Jurmeister, M. Baumann, A. Balwierz, I. Keklikoglou, A. Ward, S. Uhlmann, J. D. Zhang, S. Wiemann and Ö. Sahin, *Mol. Cell. Biol.*, 2012, **32**, 633–651.
78 M. Brentnall, L. Rodriguez-Menocal, R. L. De Guevara, E. Cepero and L. H. Boise, *BMC Cell Biol.*, 2013, **14**, 32.
79 K. Kashima, H. Kawauchi, H. Tanimura, Y. Tachibana, T. Chiba, T. Torizawa and H. Sakamoto, *Mol. Cancer Ther.*, 2020, **19**, 2288–2297.
80 J. Stamos, M. X. Sliwkowski and C. Eigenbrot, *J. Biol. Chem.*, 2002, **277**, 46265–46272.
81 N. I. Mansour, S. M. El-Sayed, N. S. El-Gohary, N. I. Abdel-Aziz, H. I. El-Subbagh and M. A. Ghaly, *Bioorg. Chem.*, 2022, **127**, 105966.
82 T.-H. Wang, Y.-L. Leu, C.-C. Chen, H.-J. Li, S.-C. Yang, K.-Y. Huang and C.-Y. Chen, *Phytother. Res.*, 2022, **36**, 2116–2126.
83 T. Jiang, Y.-D. Zhang, Q. Gao, J.-S. Zhou, X.-C. Zhu, H. Lu, J.-Q. Shi, L. Tan, Q. Chen and J.-T. Yu, *Acta Neuropathol.*, 2016, **132**, 667–683.
84 Y.-H. Yeh, C.-Y. Liang, M.-L. Chen, F.-M. Tsai, Y.-Y. Lin, M.-C. Lee, J.-S. Wu and C.-Y. Kuo, *Food Sci. Nutr.*, 2019, **7**, 1891–1898.
85 P. Labute, *Proteins*, 2009, **75**, 187–205.